1 INTRODUCTION

Adapted with permission from Hunter, B. M.; Gray, H. B.; Müller, A. M. Earth-Abundant Heterogeneous Water Oxidation Catalysts. *Chemical Reviews* **2016**, *116*, 14120. DOI: 10.1021/acs.chemrev.6b00398.

1.1 Purpose and Scope

The development and characterization of the nickel-iron layered double hydroxide ([NiFe]-LDH) water oxidation catalyst forms the central theme of my graduate work and this thesis. Our understanding of this system developed rather linearly, and so this document is ordered nearly chronologically. Each chapter is designed to be self-contained; as such, there is no separate methods chapter. I hope that researchers interested in solar fuel generation will find this organization helpful as they design novel experiments.

Chapter 1 provides an introduction to earth-abundant heterogeneous water oxidation catalysts, highlighting recent advances made in the field. It also gives some biologically relevant background that I believe may be important mechanistically moving forward. Because our initial goal was to develop a solar-driven device for the synthesis of fuels, the focus is on hydrogen production.

In Chapter 2, the synthesis of the [NiFe]-LDH catalyst is reported. This catalyst displays the lowest overpotential (the difference between the thermodynamic potential for water oxidation and the experimental potential required to reach a specified current density, in our case always 10 mA/cm^2) to date on a flat electrode. Specific details regarding the pulsed laser synthetic technique are given.

Our first mechanistic study is recounted in Chapter 3, where the effects of interlayer anions are explored. Here, catalyst performance was assessed for different intercalated anions, and the "nitrate effect" in the X-ray photoelectron spectroscopy was explained by computational chemistry.

The vast majority of my graduate career was spent collecting the data appearing in Chapter 4, which represents a detailed spectroscopic study of intermediates accessible under high potentials in non-aqueous media. These experiments represent a new paradigm for studying water oxidation catalysts in which the substrate (i.e. water) is withheld and reintroduced strategically to close the catalytic cycle. Here, details of an unusual *cis*-dioxo iron(VI) active species are elucidated, and a mechanism for water oxidation in base is proposed.

Chapter 5 represents a broadening of our initial goal by incorporating new substrates for the reductive half-reaction. These studies are mostly preliminary, but show that fuels are only the beginning of the important value-added products accessible by sunlight/water conversion.

Finally, in Chapter 6, I have attempted to look ahead at the future of heterogeneous water oxidation catalysts and make some predictions based on my experiences and theory. I hope these observations will be useful to researchers in the field.

I have also included Appendix A, which is thematically linked to the main text; these experiments involve water oxidation in living cartilaginous tissue. Many of the lessons learned in Chapters 1-6 are applicable.

Appendices B-D are superficially unrelated to the remainder of the thesis, but tell a cohesive story in themselves. A case study in binuclear d^8-d^8 complexes, these experiments represent the first and last that I have performed as a graduate student.

My hope is that this repository of my time at Caltech will be useful to those who wish to follow up on the work I have done, whether in the Gray Group or elsewhere. Many of these projects I expect to continue to work on, so this thesis is, in some ways, a mechanism of closure for the "early days." I look forward to continued spirited discussions about these results.

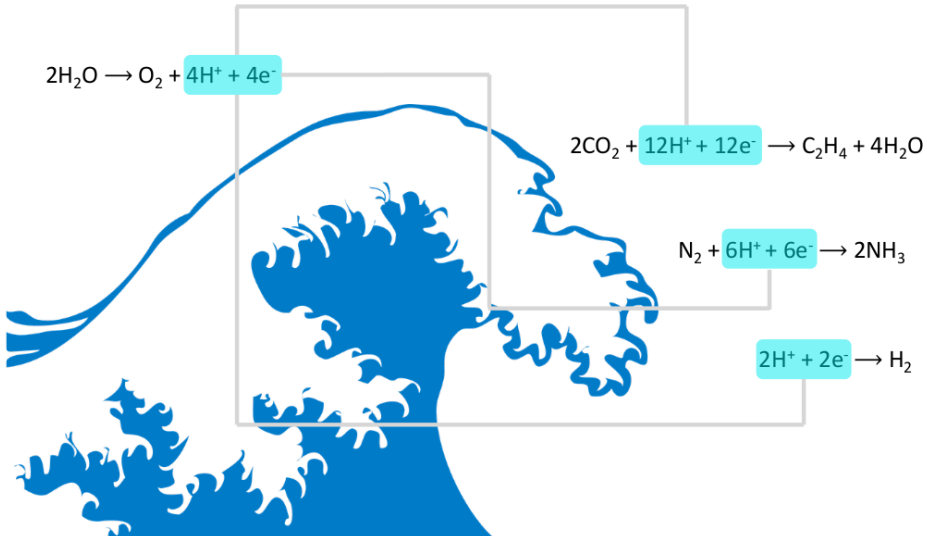

Figure 1.1. The water oxidation half-reaction provides protons (H+) and electrons (e-), which can be used to reduce a variety of abundant feedstocks to make fuels (e.g. hydrogen) and materials (e.g. ethylene and ammonia).

1.2 Why Water Oxidation?

The oxidation of water to oxygen liberates the protons and electrons required for the generation of fuels and other valuable molecules (Figure 1.1). Much progress has been made recently in designing and synthesizing scalable, heterogeneous water oxidation catalysts for solar-driven water splitting. Here, we provide an outlook on the future of such materials, with an eye toward rational design of high-performing catalysts.

The development of renewable energy systems is the greatest challenge for humanity in the 21st century.[1] All aspects of life on our planet depend on the global availability of clean and affordable energy. It is cause for concern that power consumption on earth (~13.5 TW in 2001) is expected to double by 2050 and triple by 2100.[2] We must call on the sun for survival: it is by far our largest and most reliable source of energy; it delivers an entire year's worth of energy to the earth's surface within 80 min.[3]

As fossil fuels have high energy density, we have become reliant on them for most of our needs. However, combustion of fossil fuels has detrimental effects on climate and health. In addition to global climate change attributable to rapidly increasing CO_2

concentrations in the atmosphere, excessive emissions that form smog have become a big problem in many countries. Furthermore, the dependence of industrialized nations on oil, gas, and coal and the ever-increasing demand for energy are roadblocks in efforts for world peace.[4] A paradigm shift in our current infrastructure is needed to avoid catastrophe.[5]

Fossil fuels are byproducts of eons of photosynthesis.[6] The issues we are encountering from their use arise from the large amount we combust in the relatively short timeframe of a few centuries. In light of the devastating effects and even more alarming prospects of air pollution and climate change, the need for viable energy solutions that do not interfere with our lifestyle has never been more urgent. The fight against global warming has begun, and significant amounts of funding have been pledged to combat it.[7] Yet, as developing nations become more prosperous and technology advances, worldwide demand for energy will continue to increase. This dilemma can only be solved by innovation: we will focus on earth-abundant materials tailored for carbon-neutral fuel generation, as these could lead to technologies to solve problems associated with the energy and concomitant climate crisis.

1.2.1 Potentials of Water Splitting Reactions

An attractive, carbon-neutral solution is solar-driven water splitting to produce hydrogen fuel from water[1] (Figure 1.2). All the materials needed for efficient water splitting must consist of earth-abundant elements to achieve global scalability.[8]

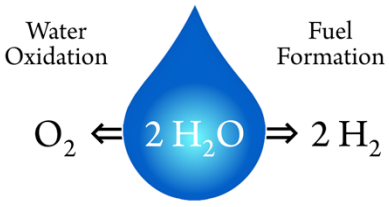

Figure 1.2. Schematic of water splitting.

The thermodynamic potential of the water splitting reaction, $2H_2O(l) \rightarrow 2H_2(g) + O_2(g)$, is $\Delta E^0 = -1.23$ V. The stepwise oxidation of water requires large overpotentials. The

overpotential of a redox reaction is the potential above the thermodynamic potential needed to overcome reaction barriers; in electrocatalysis, it is referenced to a given turnover frequency or current density. At all pH values, the standard potential for the four-electron, four-proton oxidation of water is substantially lower than that for some of the sequential one-electron steps. At pH 7, the one-electron reduction potential for the hydroxyl radical ($^{\bullet}$OH) is 2.32 V, over 1.5 V more positive than the reduction potential for the four-electron concerted reduction of dioxygen (0.815 V at pH 7).[9]

In nature, water oxidation is accomplished by photosystem II (PS II), the highly-conserved machinery for the production of plant fuel from sunlight. The water-oxidizing complex (WOC) is an inorganic calcium-manganese-oxo cluster,[10] whose structure has been studied extensively by X-ray crystallography.[11] Of critical importance is that water oxidation is carried out in a series of proton-coupled electron transfer (PCET) steps.[12] The so-called "Kok cycle" of the WOC dictates that one proton leaves the reaction center for each electron that leaves.[13] The resulting effect is a "potential leveling" scheme in which subsequent oxidation steps take place at potentials similar to the first. In the absence of PCET, charge-build up on the WOC would necessitate prohibitively high potentials for the second, third, and fourth oxidation steps.[14] A theoretical framework for PCET has been developed by Cukier[15,16] and Hammes-Schiffer.[17,18] There has been much recent work on synthetic analogues of the WOC.[19-22] In one study of note, Agapie and coworkers found that redox inactive metals modulated the reduction potentials of the Mn ions in their clusters.[23]

Depending on solution pH, water splitting proceeds by different half reactions (Figure 1.3). In aqueous acid (pH 0), the water oxidation half reaction has $E^0 = 1.23$ V, while the proton reduction half reaction has $E^0 = 0.00$ V (by modern convention, all half reaction potentials are given as the reduction potentials). At pH 14, E^0 is 0.83 V for the hydrogen evolution half reaction and 0.40 V for the water oxidation half reaction. These potentials are milder relative to the normal hydrogen electrode, which could have implications on catalyst stability and device design. It is worth noting that dioxygen reduction may compete with proton reduction under acidic conditions.

In aqueous acid:

$$2\,H_2O\,(l) \rightarrow O_2\,(g) + 4\,H^+ + 4\,e^- \qquad -E^0 = -1.23\ V$$
$$4\,H^+ + 4\,e^- \rightarrow 2\,H_2\,(g) \qquad E^0 = 0.00\ V$$
$$2\,H_2O\,(l) \rightarrow O_2\,(g) + 2\,H_2\,(g) \qquad \Delta E^0 = -1.23\ V$$

In aqueous base:

$$4\,OH^- \rightarrow O_2\,(g) + 2\,H_2O\,(l) + 4\,e^- \qquad -E^0 = -0.40\ V$$
$$4\,H_2O\,(l) + 2\,e^- \rightarrow 2\,H_2\,(g) + 4\,OH^- \qquad E^0 = -0.83\ V$$
$$2\,H_2O\,(l) \rightarrow O_2\,(g) + 2\,H_2\,(g) \qquad \Delta E^0 = -1.23\ V$$

Figure 1.3. Water splitting half reactions at low and high pH.

1.2.2 Solar Water Splitting Device Designs

Designs of solar-driven water splitting devices come in three flavors.[24] Photovoltaic–electrolyzer combinations are most mature technologically but could be surpassed by fully integrated wireless devices. Photocatalyst colloids, where the oxygen and hydrogen evolution reactions (OER and HER) occur together, have issues with the formation of explosive H_2 and O_2 mixtures. The integrated photoelectrochemical (PEC) devices, also called tandem or monolithic devices, strike a balance between the two limits. They are wireless to avoid ohmic losses, and the components for light capture and catalysis, as well as for OER and HER are separated. Decoupling the processes of light capture and catalysis offers advantages, because size matters. Optimal dimensions for light absorbers are typically on the order of a hundred nanometers. For catalysts, however, smaller is better, as chemical (redox) reactions occur on a molecular scale. Shrinking catalyst size provides more active surface sites per mass because the surface-to-volume ratio changes favorably as particles get smaller. Several investigators have discussed the advantages and disadvantages of various photoelectrochemical device designs.[25-37]

Irrespective of device design, water oxidation catalysis is crucial for harnessing solar photons. Not only water splitting but also other green chemistry transformations require the electrons and protons generated by the oxidation of our most abundant feedstock. As recent reviews summarized the design criteria and reactivities of molecular catalysts,[38-40] we focus here only on heterogeneous catalysts.

1.2.3. Materials Stability Considerations

Electrochemical equilibria of metals in aqueous solutions are well described in the Pourbaix Atlas.[41] The data compiled in this atlas show that, at high potentials, more stable earth-abundant metal oxide or hydroxide materials exist in high pH electrolyte (Figure 1.4). Anion exchange membranes (AEMs) are currently being developed to replace Nafion® as the separator between the oxygen and hydrogen evolving compartments of a tandem device.[42,43] Devices typically operate at extreme pH, *i.e.* strong aqueous base or acid.[44] It is not clear at this time if overall acidic or alkaline conditions will work better for water splitting devices, given the requirements of scalability, efficiency, and robustness.[45]

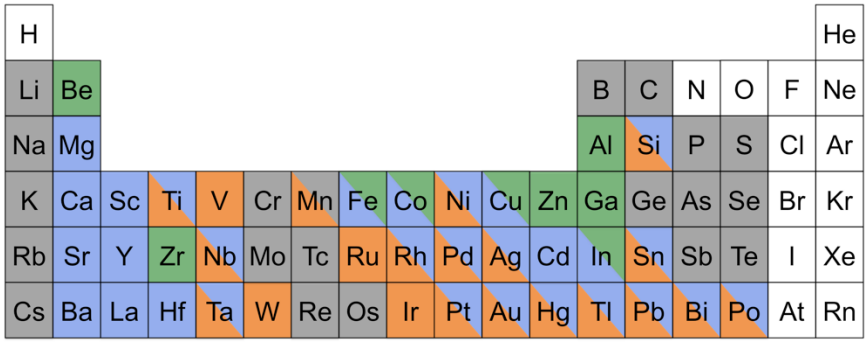

Figure 1.4. Corrosion stability of non-gaseous group 1 through 16 elements for element–water systems at 25°C under positive applied potentials, adapted from the Pourbaix Atlas.[41] Color code: stable against corrosion by innate immunity or the formation of an oxide or hydroxide layer at low (orange), around neutral (green), and high (blue) pH. Elements that corrode under applied oxidative potentials are depicted in gray. Multiple colors (blue/orange, blue/green) indicate stability over a wide pH range. The combination orange/gray is for stability at low pH but only for moderately positive potentials.

Since we know that water oxidation catalysts will be required to operate at high potentials, we have color-coded the non-gaseous group 1 through 16 elements of the periodic table that are corrosion-resistant by innate immunity or the formation of an oxide or hydroxide layer at different pH values in water (based on data from the Pourbaix Atlas;[41] Figure 1.4). Elements that are stable against corrosion under applied anodic potential and low pH are colored orange. Those that are immune to corrosion at neutral pH are depicted in green, and those that are stable at high pH are in blue. Elements that always corrode under

high anodic potentials are gray. We believe that this chart could serve as a roadmap for the development of stable water oxidation catalysts, although it should be noted that it does not take into account mixtures or alloys.

Of interest is that bismuth vanadate is stable in base, even though vanadium is orange in the table; vanadate ions by themselves are stable at high pH under anodic polarization.[41] Other binary systems show similar behavior that deviates from simple Pourbaix predictions. Although manganese is not stable in 0.1 M aqueous KOH, the $Ca_2Mn_2O_5$ oxygen-deficient perovskite is a stable water oxidation catalyst under these conditions.[46] Another strategy involves mixing base-unstable metals into nickel-containing double hydroxides. OER catalysts based on nickel double hydroxides and Cr, Mn, or Zn are stable in 0.1 M aqueous KOH even though Cr, Mn, and Zn are not independently stable in base.[47] Ternary systems also have been explored, with the perovskites $LaCrO_3$, $La_{0.7}Sr_{0.3}CrO_3$, and $La_{0.8}Sr_{0.2}CrO_3$ being stable for OER in 1 M aqueous NaOH, contrary to the prediction for Cr.[48]

Commercial water electrolyzers consist of OER and HER catalysts, and the two half reactions are separated by a membrane.[49] In high current-density systems, both catalysts are based on scarce metals, Pt for HER and IrO_2 for OER.[50] Noble metal oxides (Rh, Ir, Ru) were identified as highly active heterogeneous catalysts for water oxidation.[51] Iridium oxide (IrO_2), though not earth-abundant, was subsequently found to be one of the most active materials.[52] Further investigations demonstrated that molecular precursors can form highly active heterogeneous catalysts based on iridium oxide.[53] In related work, a quartz crystal microbalance was employed to differentiate between homogeneous and heterogeneous iridium catalysis.[54] Interestingly, Osterloh *et al.* used iridium dioxide nanocrystals as both photoanode and catalyst to split water with visible and UV light,[55] and iridium-doped metal-organic frameworks were found to be competent for water oxidation.[56] Iridium-based catalysts will not be able to provide a globally scalable solution to our energy problem because Ir is the scarcest element in earth's upper crust.[8]

1.3 Earth-Abundant Water Oxidation Catalysts

In 1972, Fujishima and Honda showed that TiO_2 was capable of splitting water as both a photoanode (light absorber providing holes, h^+) and water oxidation catalyst.[57] Although TiO_2 is not an efficient catalyst for water oxidation and its large bandgap E_g of >3.0 eV[58] limits its overlap with the solar spectrum, the use of semiconductors to absorb visible light to effect water oxidation was an important development. Even though TiO_2 has been studied intensely the past few decades, attempts to substantially enhance its light absorption properties have not met with much success.[59]

Other metal oxides, such as ZnO,[60] La:$NaTaO_3$,[61,62] WO_3,[63,64] and $SrTiO_3$,[65] have been investigated for solar-driven water splitting. All these materials have bandgaps that are too large to make good use of sunlight, thereby limiting overall solar-to-hydrogen efficiencies.[66] A few visible-light absorbers have been examined. Shifting the absorption edge of TiO_2 toward the visible region was achieved by nitrogen doping, which turned the material yellow (E_g = 2.9 eV).[67] And molecular nitrogen-intercalation decreased the bandgap of WO_3 to 1.9 eV.[68] Nevertheless, neither material met all the requirements for efficient water oxidation.[69] Shao-Horn *et al.* predicted and experimentally confirmed OER activity of a complex Ba-Co-Sr-Fe (BCSF) oxide perovskite material that compared favorably with IrO_2.[70] Electronic structure−activity relationships in similar perovskites were reported.[71] Combining a co-catalyst with active photoanode materials has become the most promising methodology, evidenced by recent work by Marschall *et al.* on layered perovskite nanofiber photoanodes with photodeposited Rh-Cr_2O_3.[72]

Bismuth vanadate ($BiVO_4$) has been identified as a promising photoanode material for solar water oxidation.[73] It has been shown to be stable against photocorrosion in aqueous electrolytes from pH 3 to 13.[74] $BiVO_4$ crystallizes in different polymorphs, with monoclinic scheelite exhibiting the highest photocatalytic water oxidation activity.[75,76] This crystalline phase of $BiVO_4$ is an *n*-type semiconductor with a direct bandgap of 2.4 eV (making it appear yellow) and a valence band edge at ~2.4 V vs. RHE (reversible hydrogen electrode) that is sufficiently positive to effect water oxidation.[58,77] Water oxidation efficiency is mainly

limited by high electron-hole recombination, inadequate water oxidation kinetics, and poor charge transport properties.[73]

Large variations of photocurrents have been reported for $BiVO_4$ photoanodes.[78-87] In recent work, we correlated morphology and chemical surface composition of this material to its photoelectrochemical performance, with the aim to differentiate contributions from different properties.[88] We devised a novel anodic electrodeposition procedure with different amounts of iodide added to the aqueous plating bath, which allowed us to prepare $BiVO_4$ films with virtually identical thicknesses but different morphologies, and we could control surface Bi content (Figure 1.5).[88]

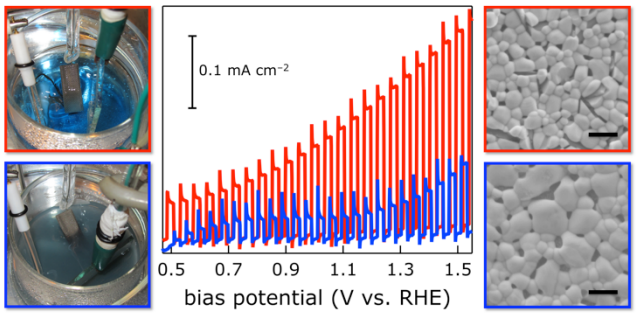

Figure 1.5. Effect of $BiVO_4$ preparation conditions on photocurrent generation (blue, without, red, with iodide in the electrodeposition bath).[88] Left: Photos of the plating baths, center: measured chopped-illumination photocurrent densities as a function of bias potential vs. the reversible hydrogen electrode (RHE), right: SEM images of the resulting $BiVO_4$ photoanodes; the scale bars are 1 μm. Experimental details are given in ref. 88.

Optimized photocurrent generation of $BiVO_4$ photoanodes resulted from intertwined material properties, whose interplay was probed by bivariate data analysis. Our data showed that a near-stoichiometric surface Bi/V ratio in combination with high-aspect-ratio crystallites, which were small enough to provide efficient charge separation yet sufficiently large to overcome mass transport limitations, led to highest photocurrent generation.[88]

1.3.1 Water Oxidation Catalysts Based on First-Row Transition Metals

Bio-inspired manganese oxides have also received considerable attention. In 1977, Morita *et al.* discovered that MnO_2 electrocatalytically evolved O_2 in alkaline aqueous electrolyte.[89] Later, Harriman *et al.* observed Mn_2O_3-catalyzed water oxidation.[51] Frei *et al.* reported water oxidation catalysis by various nanostructured Mn oxides on mesoporous silica supports, with Mn_2O_3 exhibiting highest activity.[90] Jaramillo *et al.* identified layered Na-birnessite MnO_2 as an oxygen-evolving photoanode material.[91] Dau and Kurz *et al.* prepared birnessite Mn oxides with intercalated divalent cations; they found a $Ca^{2+} > Sr^{2+} > Mg^{2+}$ order for catalytic activities.[92] Stahl *et al.* reported that activities of Mn oxides depended on the choice of oxidation method.[93] Many different Mn oxide precatalysts converted into layered structures under OER conditions, as predicted by the Mn–H_2O Pourbaix diagram.[41,94] Dau and coworkers found that cyclical electrochemical deposition of MnO_2 produced Mn^{III} sites that were active for water oxidation at pH 7.[95] Further, it was shown[96] that as-prepared α-Mn_2O_3 and Ca–Mn^{III} oxide hydrates, $CaMn_2O_4{\cdot}xH_2O$, catalyzed water oxidation in the presence of either Oxone®,[97] a two-electron oxygen-transfer oxidant (HSO_5^-), or Ce^{IV}, a one-electron oxidant. As with molecular iridium precursors, Zaharieva *et al.* found that the binuclear manganese complex $[(OH_2)(terpy)Mn(\mu\text{-}O)_2Mn(terpy)(OH_2)]^{3+}$ (terpy is 2,2';6',2''-terpyridine) was transformed into layered Mn oxide particles on clay, which served as the active water oxidation catalyst.[98] In other work of note, Jaramillo *et al.* prepared nanostructured Mn^{III} oxides that showed activity similar to noble metals for both water oxidation and oxygen reduction.[99,100]

Iron oxide water oxidation materials have been heavily studied. Iron oxides are appealing materials for globally scalable, clean energy conversion applications because of the abundance and low cost of iron. Somorjai *et al.* determined that the active optical component of an iron oxide electrode is α-Fe_2O_3.[101] Iron(III) oxide showed excellent long-term stability, but had low efficiency (0.05%) for solar conversion to H_2 and O_2.[101] The very short hole lifetime of hematite (a few picoseconds)[102] presents a major obstacle. Berlinguette *et al.* found that amorphous Fe_2O_3 showed improved water oxidation activity.[103] By doping Fe_2O_3 with silicon, Grätzel *et al.* were able to increase the conversion efficiency to a

theoretical 2.1% in a tandem device.[104] Detailed electrochemical studies on passivated iron oxide electrodes by Lyons *et al.* suggested that a physisorbed peroxide pathway is dominant and that the active site is a stabilized Fe^{VI} species.[105]

Cobalt oxide (CoO_x) is stable only at high pH under positive potentials.[41] Yet Nocera *et al.* found that a heterogeneous catalyst based on Co^{II} phosphate (CoP_i), which had been formed *in situ* during electrodeposition on indium tin oxide, was highly active for water oxidation and virtually indefinitely stable in phosphate buffer at pH 7.[106] Further work on this system demonstrated that Co^{IV} was generated at potentials at which water oxidation occurred.[107] Dau *et al.*, who found that all cobalt oxide films active for water oxidation featured edge-sharing CoO_6 octahedra, concluded that O–O bond formation occurred at the edges of the cobalt oxide clusters.[108] They noted that there is no specific "recipe" for synthesizing a catalyst that works, *e.g.* specific anions or redox-inactive cations, but that these factors play a large role in determining size and potential.

Cobalt-oxide water oxidation catalysts have received attention for more than 65 years. Initial electrochemical characterization of the behavior of cobalt metal in alkaline conditions indicated that three oxides, namely CoO, Co_2O_3, and CoO_2, were accessible under anodic bias.[109] The development of alternative structures, such as Co_3O_4, has shown increased promise (there has been success incorporating Co_3O_4 in a silica scaffold).[110] Two polymorphs of lithium cobalt oxide were synthesized by Dismukes *et al.*, and it was determined that the presence of a Co_4O_4 cubic core was indicative of water oxidation activity.[111] (We note that this cubane motif is present in PS II, albeit with manganese instead of cobalt.) Cobalt-manganese hydroxide was more active than the respective single-metal oxides.[112] Wang and coworkers were able to synthesize size-controlled Co_3O_4 nanoparticles without supporting ligands, and found that both size control and the absence of ligands that prevented species from diffusing to the surface were essential for activity.[113] In an electrochemical study, Lyons *et al.* concluded that Co^{IV} was the active species.[114]

We employed pulsed laser ablation in liquids (PLAL) as a technique for the synthesis of surfactant-free, size- and composition-controlled <5-nm cobalt oxide nanoparticles.[115] In PLAL, a high-energy laser pulse is focused on a solid target that is submerged in liquid. The pulse creates a plasma plume, which is confined at xshigh temperature and pressure by the

liquid. Extreme pressure triggers a shock wave in the confining liquid, causing the plasma to rapidly expand and cool. Nanoparticles condense out and are injected into the surrounding liquid. Our Co_3O_4 nanoparticles synthesized by PLAL had an overpotential for water oxidation of 314 mV (measured at 0.5 mA cm^{-2}), comparing favorably with the best electrodeposited cobalt oxide species; our material also featured very high mass activity of more than 10 A m^{-2} g^{-1} at 500 mV overpotential (Figure 1.6).[115]

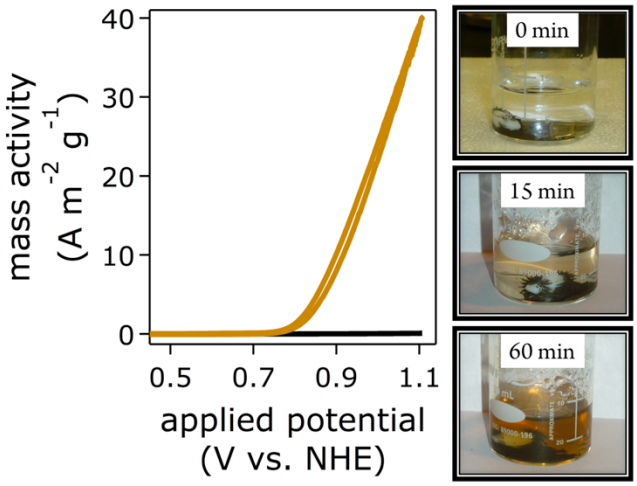

Figure 1.6. Left: Mass activity for water oxidation in 1.0 M aqueous KOH on flat graphite electrodes as a function of applied potential vs. the normal hydrogen electrode (NHE); yellow, Co_3O_4 nanoparticles synthesized by PLAL at 90 mJ $pulse^{-1}$, black, commercial 50-μm-diameter Co_3O_4 powder. Right: PLAL preparation of Co_3O_4 nanoparticles from Co powder in water at different synthesis durations.

Another first-row transition metal oxide, NiO_x, which was identified as a water oxidation catalyst by Bode in 1966,[116] was studied in depth in the 1980's.[117] Soon it was discovered that even tiny amounts of iron improved the water oxidation activity of NiO_x.[118,119] In a thorough study of iron incorporation into nickel oxide films, Boettcher *et al.* found that even accidental incorporation of iron enhanced catalytic activity.[120] Electrochemical investigations of nickel oxide electrodes by Lyons *et al.* concluded that the likeliest mechanisms involve Ni^{III} or Ni^{IV}, again in a physisorbed peroxide scheme. Lyons *et al.* did not invoke multiple oxidation states of nickel, instead using the electrode as the hole (h^+) acceptor throughout.[121] In other work, Stahl *et al.* synthesized an inverse spinel

$NiFeAlO_4$ material that had an overpotential for water oxidation of 330 mV at 0.5 mA cm^{-2} per active nickel.[122] Interestingly, the addition of a redox-inert metal enhanced the water oxidation activity of this material.

The effect of scandium on electrodeposited NiP has been explored.[123] Briefly, increasing the Sc_2O_3 composition in an amorphous NiP layer lowered the overpotential for water oxidation up to an ideal concentration of ~10%. Above ~10%, a decrease in activity was observed.

Very few vanadium-only materials have been tested for water oxidation activity. Binary and tertiary materials have been the primary focus, likely because of poor performance of vanadium oxide alone. Bismuth vanadate has been employed as a photoanode, as previously discussed; it also is catalytically active. Kudo *et al.* synthesized bismuth vanadates with varying V:Bi ratios and crystal forms that showed oxygen evolution rates from 2.5-421 μmol h^{-1} (the best performing material was in the monoclinic crystal form) under visible light irradiation.[75] The addition of copper ($BiCu_2VO_6$) reduced the bandgap, allowing greater absorption of visible light.[124] Finally, the addition of a more active metal, such as cobalt, has been shown greatly to increase the activity of vanadium-based catalysts, and binary nanoparticles, such as $Co_3V_2O_8$, have improved performance.[125]

Several chromium-based catalysts have been screened for water oxidation activity. Bockris and Otagawa measured current density in terms of real surface area for a number of perovskites at 0.3 V overpotential.[48] They found that the $La_{0.8}Sr_{0.2}CrO_3$ perovskite only passed 3.2×10^{-8} A cm^{-2}, the lowest value observed with the exception of $LaVO_3$. Solid Cr_2O_3 also has been employed as a water oxidation catalyst under supercritical conditions, with the active species believed to be chromic acid, H_2CrO_4.[126] On the other hand, small amounts of Cr_2O_3 on a $Ba_5Ta_4O_{15}$ perovskite surface produced a stable photoanode, with an oxygen evolution rate of 228 μmol h^{-1} when illuminated with a 500 W Hg immersion lamp.[127]

Copper-based water oxidation catalysts have recently attracted attention. Meyer *et al.* synthesized transparent and flexible Cu/CuO nanowire films that were active for water oxidation.[128] The CuO film prevented electrochemical corrosion of the material, although the overpotential was 580 mV at 10 mA cm^{-2}. Other groups have reported using $Cu(OH)_2$ as an inexpensive, earth-abundant material for water oxidation in base, but with similarly high

overpotentials.[129] Recently, the performance of Cu-based catalysts has been dramatically improved by *in-situ* generation of copper oxide films from a copper(II) ethylenediamine complex.[130] A current density of 10 mA cm^{-2} was obtained at an overpotential of ~475 mV in 1.0 M aqueous KOH. It also has been shown that the extent to which copper complexes perform water oxidation homogeneously *vs.* heterogeneously is pH dependent.[131] Functioning photoelectrochemical (PEC) devices have been fabricated with copper oxide/silicon photoanodes, showing good stability and electrocatalytic behavior.[132] The current work on copper-based catalysts is encouraging, but the electrocatalytic activities of these materials remain far inferior to Fe, Co, and Ni based systems.

Zinc oxide (ZnO) nanowire arrays exhibit moderate photocurrent density (0.62 mA cm^{-2} at 1.0 V *vs.* RHE under 1 sun illumination) but can be improved by the addition of Co-P_i or Ni-B co-catalysts.[133] Importantly, these materials are very stable to corrosion, showing no loss in photocurrent over prolonged testing. Choi *et al.* synthesized a spinel-type $ZnCo_2O_4$ thin film that showed a relatively low overpotential (390 mV at 10 mV cm^{-2}).[134] Although this finding underscored the advantage of incorporating more active metals, the resulting material is more active than that of Co_3O_4 electrodes prepared from the same synthesis conditions with comparable thickness and morphology. It is unclear whether zinc is playing a direct role in catalysis or simply in tuning the redox potential of the cobalt material. Similarly, it has been shown that the overpotential of ZnO can be lowered by doping with Mn, Fe, Co, and Ni.[135] The largest effect (by almost 150 mV) was seen with cobalt doping.

In other work of note, polyoxometallates based on first-row transition metals have been shown to act as heterogeneous water oxidation catalysts.[136,137] Polyoxometallates (POMs) are polyoxoanions that can contain between 5-50 transition metal centers. Because of their unusual oxidative stability, high-valent states of the metal atoms are accessible (e.g. Ni^{IV} and Cr^{V}).[138,139] Although most clusters are generally believed to be active in homogeneous solutions, Co_4POM has been shown to be a precursor to an active heterogeneous CoO_x catalyst. Other researchers have utilized POM frameworks to synthesize mesoporous structures of first-row transition metal oxides, such as Co_3O_4.[140] These types of hybrid materials are promising water oxidation catalysts.[141]

Among first-row transition metals, cobalt, iron, and nickel oxides and hydroxides are most active for water oxidation, at least in alkaline electrolytes. Because higher electrocatalytic activities have been observed in layered double hydroxides, we turn our attention to this class of materials.

1.3.2 Layered Double Hydroxides

Much recent research has focused on layered double hydroxides (LDHs), mineral-like compounds that contain a sheet of $M_1^{2+}(OH)_6$ shared-edge octahedra with M_2^{3+} atoms occupying some of the M_1 sites.[142,143] Intercalated anions balance the additional positive charge of M_2^{3+}, while layers between sheets carry water. Dai *et al.* demonstrated that a composite of α-$Ni(OH)_2$ on carbon nanotubes was efficient for water oxidation.[144] Nickel-titanium LDHs were shown by O'Hare *et al.* to be very active photocatalysts.[145]

Based on previous work on iron-doped nickel oxides, [NiFe]-LDH materials have become a target for many groups. Boettcher *et al.* suggested that layered structures are particularly useful for highly efficient water oxidation catalysis.[146] Exfoliation of [NiFe]-LDHs into individual layers led to increased water oxidation activity.[147] Other iron-containing LDHs, [MFe]-LDH nanoplatelet arrays where M is Ni, Co, or Li, have been prepared by short-time electrodeposition on foam nickel substrates; all OER overpotentials were assessed on rough supporting electrodes of unknown microscopic area.[148]

We used PLAL to synthesize [NiFe]-LDH nanosheet water oxidation catalysts.[149] The x-ray diffraction (XRD) patterns of our materials were characteristic of layered double hydroxides, since the intensities of the basal (00*l*) reflections decreased as *l* increased.[150] The observed reflections were indexed in a three-layer **3R** polytype with rhombohedral symmetry, such as in synthetic hydrotalcite (Figure 1.7).[151] The XRD data of LDH materials provide rich information on the basal spacing, the interlamellar electron density stemming from interlayer water and anions, and the nanosheet size, *i.e.* lateral diameter and stack thickness.[150]

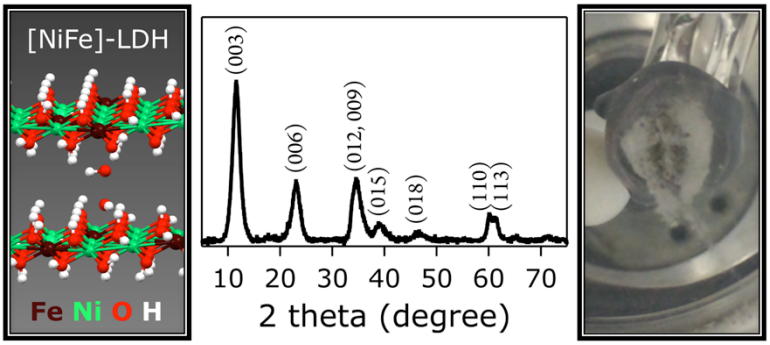

Figure 1.7. Left: Schematic illustration[152] of the structure of [NiFe]-LDH nanosheet water oxidation catalysts.[149] Center: Indexed XRD data that evidence the layered double hydroxide structure of our materials. Right: Photo of [NiFe]-LDH nanosheets during water oxidation catalysis under anodic bias in aqueous alkaline electrolyte.

The [NiFe]-LDH nanosheet water oxidation catalysts synthesized by PLAL showed outstanding performance on flat graphite electrodes; the best catalyst had 260 mV overpotential at 10 mA cm^{-2}.[149] Overpotentials of earth-abundant catalysts at 10 mA cm^{-2} typically range from 350 to 430 mV in pH 14 aqueous electrolytes[153] (Figure 1.8). We note that McCrory tested the activities of our PLAL-made Co_3O_4 water oxidation catalysts and confirmed the overpotentials we had reported.[115] His findings suggest that our overpotential assessment method was equivalent to the benchmarking technique reported by McCrory, Peters, Jaramillo, *et al.*,[153] indicating that electrocatalytic activities of different materials are directly comparable between the two laboratories.

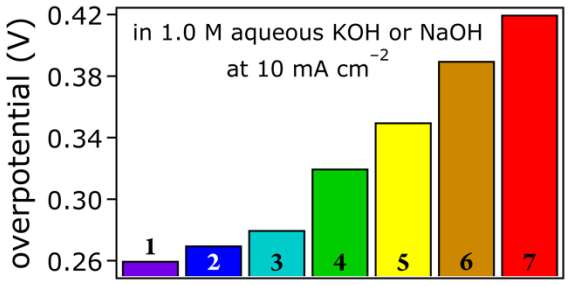

Figure 1.8. Comparison of overpotentials of our (1 to 3)[149] and other (4 to 7)[153] reported water oxidation electrocatalysts operating in 1.0 M aqueous base. The materials are Ti and La doped [NiFe]-LDH nanosheets (1), Ti doped [NiFe]-LDH nanosheets (2), [NiFe]-LDH nanosheets with 22% Fe (3), IrO_x (4), $NiFeO_x$ (5), CoO_x (6), and NiO_x (7).

Other nickel-based materials have been reported with overpotentials at current densities other than 10 mA cm^{-2}, rendering a direct comparison problematic. Adventitious nickel at concentrations as low as 17 nM was shown to catalyze water oxidation in aqueous electrolytes, with stable (tens of hours) current densities of 1 mA cm^{-2} at overpotentials as low as 540 mV at pH 9.2 and 400 mV at pH 13.[154] Thin film nickel oxide with iron impurities reached 8 mA cm^{-2} at 230 mV,[119] while β-NiOOH exhibited an overpotential of 500 mV at a current density of 5 mA cm^{-2}.[155] Nickel-borates on glassy carbon and mixed Fe-Ni oxides on carbon paper reached 1 mA cm^{-2} at overpotentials of 425 and 375 mV, respectively.[156,157] Amorphous α-$Fe_{20}Ni_{80}O_x$ on FTO glass had an overpotential of 210 mV at 0.5 mA cm^{-2}.[158] The same current density was reached at 265 mV overpotential by high surface-area nickel metal oxides,[159] and NiO_x deposited from molecular $[Ni(en)_3]^{2+}$ on glassy carbon featured an overpotential of 390 mV at 0.1 mA cm^{-2}.[160]

Other iron- and nickel-based catalysts showed higher overpotentials for water oxidation, or they were measured on high-surface-area electrodes, which leads to an enlargement of the electrode substrate surface area relative to the apparent geometric area, thereby inflating overpotential numbers. Thin-film solution-cast $Ni_{0.9}Fe_{0.1}O_x$ reached 10 mA cm^{-2} at 336 mV overpotential,[146] while electrodeposited $NiFeO_x$ reached the same current density at 360 mV.[153] A similar result was obtained with nanostructured α-$Ni(OH)_2$ (331 mV at 10 mA cm^{-2}).[161] With an iron content of 40%, thin-film electrodeposited Ni-Fe on gold yielded an overpotential of 280 mV.[162] A graphene FeNi double hydroxide material was reported on a nickel foam electrode with unspecified pore size and thus real electrode area.[163] Very recently, homogeneously dispersed Fe–Co–W oxyhydroxide gels were reported to have overpotentials of ≥315 mV on flat Au electrodes.[164]

1.3.3 Looking Forward

The overpotentials for water oxidation for many catalysts are within the range needed to construct viable devices, but there is still a need to optimize the photoanode/catalyst junction. Light capture in the presence of a catalyst remains a concern, since parasitic light absorption, reflection, and scattering by catalyst particles or layers reduce the efficiency of a device. In

addition, optical properties related to the size of the catalyst material become important, especially once devices become highly functional. Employing optimally sized catalyst particles may mitigate light reflection and scattering. These constraints dictate that catalyst mass activity must be high, since using less catalyst overall will improve device performance. Smaller catalysts such as nanoparticles, however, have a tendency to aggregate; methods must be developed for robust attachment under the demanding conditions of water oxidation. Clearly, it is difficult to pinpoint a common characteristic that makes earth-abundant water oxidation catalysts particularly active or inactive. We can say, however, that particle size and method of preparation are both centrally important. Ion and electron conductivity,[165] as well as carrier mobilities through the materials also matter.

1.4. Mechanistic Considerations

A major challenge is obtaining a clearer mechanistic picture of water oxidation. Elucidation of atomistic details during turnover is no easy feat, since most highly active earth-abundant heterogeneous catalysts are multi-metal materials. What is the site of catalysis? Are all metals catalytically active, or are some species simply necessary to tune the electronics of the system? What is the local structure? Are catalytic sites comprised of one or more metal centers? And are oxidized active sites electronically localized or delocalized? These questions are difficult to answer, particularly because catalytically active transient species are short-lived by definition. Experiments that detect such transient intermediates spectroscopically while the material is under positive potentials and immersed in electrolyte are badly needed.

1.4.1. Lessons from Nature

The vast body of research on photosynthetic oxygen evolution highlights the enormous scientific challenges associated with gaining mechanistic information of complex, heterogeneous systems during catalytic turnover. Nature's way of evolving oxygen in PS II

may serve as a mechanistic model for manmade heterogeneous water oxidation. But the mechanism of PS II catalysis is still hotly debated.

The first mechanistic proposal was set forth by Blackman and Matthaei in 1905, when they suggested that photosynthesis is a two-step process: a photochemical (light) reaction and a light-independent (dark) reaction that required elevated temperature and was thus indicative of an enzymatic reaction.[166] In the 1920's, Warburg observed that the rate of photosynthesis was inhibited by high oxygen concentrations and postulated that oxygen was produced from CO_2 during photosynthesis; this is known as the Warburg hypothesis.[167-169] Many scientists agreed with Warburg that the primary reaction in photosynthesis was the splitting of CO_2 by light into oxygen and carbon, which would subsequently be reduced to carbohydrates by water. Van Niel presented a fundamentally different view in the 1930's from his work on anaerobic sulfur bacteria. He demonstrated that photosynthesis is a light-driven redox reaction following the general equation of $CO_2 + 2H_2A + \text{photons} \rightarrow [CH_2O] + 2A + H_2O$, where $[CH_2O]$ is a carbohydrate and A an electron acceptor. Van Niel's discovery predicted that water is split into hydrogen and oxygen.[170] In 1937, Hill investigated the light-driven transfer of electrons from water to non-physiological oxidants in isolated chloroplasts and found that oxygen was generated in the absence of carbon dioxide.[171-173]

A major breakthrough came in 1941 at the dawn of radioisotope tracer studies, when ^{18}O labeling experiments by Ruben and coworkers established that oxygen in photosynthesis came from water rather than from carbon dioxide.[174] In addition to this landmark publication, Ruben and Kamen discovered the long-lived radioactive carbon isotope ^{14}C in 1940,[175] which paved the way for the elucidation of carbon pathways in photosynthetic metabolism by Calvin, for which he received the Nobel Prize in Chemistry in 1961. Isotope labeling studies remain some of the most powerful ways to elucidate the mechanisms of homogeneous and heterogeneous water oxidation catalysts. They allow for spectroscopic determination of intermediates and tracking of products from substrates.

By the mid 20th century, PS II was still a black box regarding its structure and molecular mechanism. Groundbreaking work by Joliot *et al.* in the 1960's established that the yield of oxygen evolution in the water splitting enzyme system follows a period-four oscillation upon irradiation with saturating light flashes.[176-178] In 1970, Kok developed a

kinetics scheme, known as the Kok or S-state cycle for PS II oxygen evolution (Figure 1.9).[13] Further insights into the mechanism of water oxidation on a molecular scale were enabled by the advent of gene sequencing and the discovery of the BBY preparation of a smaller, isolated PS II complex, which retained full activity for oxygen evolution.[179].

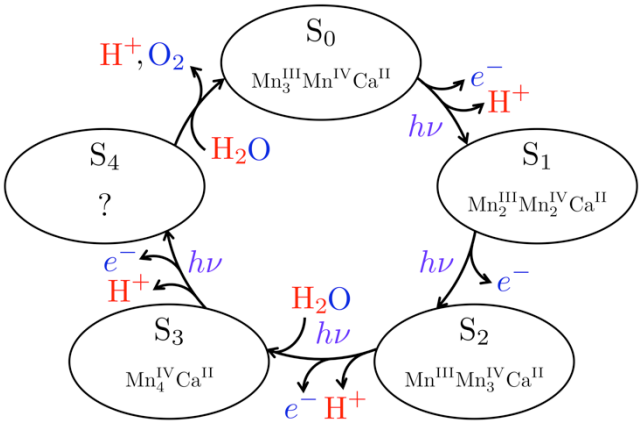

Figure 1.9. Schematic S-state cycle of the PS II WOC, including the likely oxidation states of metal ions.[13,180,181] The catalytic cycle consists of the states S_0 through S_4, where the subscript denotes the number of oxidizing equivalents abstracted from the WOC.[13] Photons ($h\nu$), electron (e^-) and proton releases, and substrate turnovers are also shown.

Great progress has been made in understanding the biochemistry of PS II, since Deisenhofer, Huber and Michel (Nobel Prize in Chemistry in 1988) determined the three-dimensional structure of a photosynthetic reaction center. Their work established the architecture of trans-membrane proteins, quinones and cytochromes. This structural information can be used analogously as the scaffold around the WOC in PS II. Work by Marcus on the theory of electron transfer reactions in chemical systems (Nobel Prize in Chemistry in 1992) inspired work by Debus, Barry, Babcock, and McIntosh in 1988, which provided the first molecular biological evidence that tyrosine radicals are involved in long-range electron transfer through P_{680}.[182,183] Importantly, the tyrosine electron carriers mediate the sequential electron transfers through the PS II protein machinery to cycle the WOC through its intermediates at moderate potentials (see section 1.2).[13,184,185]

The development of advanced electron paramagnetic resonance (EPR) and x-ray spectroscopy and diffraction techniques enabled the determination of increasingly refined

structures of the $CaMn_4O_5$ WOC.[186-189] Britt *et al.* were the first to demonstrate a $CaMn_3O_4$ cubane structure with a Mn dangler from EPR data.[190,191] Barber *et al.* obtained a 3.5 Å-resolution x-ray diffraction structure of the WOC in 2004, which confirmed Britt's cubane/Mn dangler motif, but the reported interatomic distances indicated partial reduction of the $CaMn_4O_5$ cluster by the x-ray beam.[192,193] Two years later, Messinger, Zouni, Yachandra, and co-workers examined the structure of the manganese-calcium water-splitting complex of PS II, using x-ray pulses from a femtosecond free-electron laser source; the short timescale of the x-ray pulses minimized radiation damage because diffraction data were collected before beam-induced reduction of the WOC could occur.[194] Finally, in 2011, Shen, Kamiya *et al.* reported a crystal structure of the WOC with 1.9 Å resolution and located all of the metal atoms of the Mn_4CaO_5 cluster together with all of their ligands, again verifying the Barber $CaMn_3O_4$ cube structure with a manganese dangler that is connected to the cube via an O bridge.[11]

Knowledge of the WOC structure enabled more detailed mechanistic insights into oxygen formation from water. The WOC catalyzes water oxidation to O_2 with a maximal turnover frequency of ~500 s^{-1} and a high turnover number of 10^6,[195] indicating that nature solved the difficult problems of four-electron oxidation to form molecular oxygen and simultaneous avoidance of excessive oxidative damage to the enzyme. Several key questions remained unanswered: How does the substrate for oxygen evolution bind, how does it turn over, what are the molecular intermediates? And what are the oxidation states of the individual manganese centers associated with each S state? Dismukes *et al.* established the manganese oxidation states of the S_2 state.[196] Cox, Lubitz *et al.* characterized the S_3 state (the intermediate directly prior to O–O bond formation) and reported that all manganese centers are in the IV oxidation state.[181] Three competing models predict how molecular oxygen is formed and through which pathway the S_3 state spontaneously decays to the S_0 resting state, closing the catalytic cycle.[197] Babcock proposed a metalloradical hydrogen abstraction mechanism, where S_0 is directly formed from S_3 with concomitant O_2 release.[198] Yet structural data from high-resolution x-ray experiments are not in accord with a direct O_2 generation mechanism.[11] Brudvig suggested that a single Mn^V oxo species could form an O–O bond with a Ca^{2+}-bound hydroxide or water in the S_4 transient.[199,200] But Siegbahn obtained

DFT results that favored radical O–O coupling in S_4 involving a Mn^{IV}-oxyl.[201,202] Recent work revealed that NH_3 binds at the dangler Mn site, but not in a bridging position; this finding supports both high-valent Mn–O models.[203] Molecular oxygen is released about 1 ms after the fourth photon is absorbed,[195,204] rendering structural determination of the S_4 species particularly difficult.

The lessons learned in photosynthetic WOC research should be of help in investigations of earth-abundant heterogeneous catalysts.[205] The higher stability of metal (hydr)oxide materials compared to PS II facilitates mechanistic work. Also helpful is the availability of analytical and spectroscopic methods that have been developed in the course of PS II work. Yet, even in robust materials, highly active species are short-lived and the identification of catalytic pathways remains challenging.

1.4.2. Heterogeneous Water Oxidation Catalysts

In heterogeneous catalysts, only small numbers of metal centers are active.[206] Inactive sites are likely needed to keep the material intact by providing an environment around an active site that supports high oxidation states required for water oxidation, by acting as hole reservoirs, by assisting in deprotonations, or by tuning redox potentials. Ligands assume this role in molecular catalysts, polypeptide chains in biocatalysts. In the case of water oxidation, there is intense debate if catalysis proceeds in homo- or heterogeneous fashion.[207] Robust, highly active, inorganic materials have largely regular, periodic structures, and only a few special sites are catalytically active, rendering their identification during turnover particularly challenging.

Great strides have been made with single-metal electrocatalysts, both computationally and experimentally. Rossmeisl *et al.* used density functional theory (DFT) calculations to shed light on water oxidation reactions on metal oxide surfaces that involve surface-adsorbed OOH intermediates.[208-210] Nørskov *et al.* described how computational methods provide mechanistic understanding essential for the design of new catalysts, with much emphasis on thermochemical volcano plots.[211-214] Fortunelli, Goddard, *et al.* examined OER rate-limiting steps and barriers associated with fundamental reaction steps on Pt(111)

surfaces *in silico*. They assumed a reaction pathway in which surface-adsorbed species underwent the following reactions: water dissociation, OH disproportionation, OOH formation, OOH dissociation that resulted in O_2 formation, and finally H dissolution to form an electron and solvated proton.[215] In other reports of note, Llobet *et al.* reviewed O–O bond formation pathways promoted by Ru complexes,[216] such as the "blue dimer", whose water oxidation mechanism has been studied in great detail,[217-221] and Nocera *et al.* discussed electronic design criteria for O–O bond formation *via* metal oxos.[222]

Manganese oxides support multiple metal oxidation states,[223] facilitating four-electron water oxidation. Manganese oxides occur in many different compositions and crystal phases, which affect OER activity.[224,225] Kinetics measurements on MnO_2 catalysts suggested that surface Mn^{III} sites were active.[226] The mechanism involved fast Mn oxidation coupled to deprotonation, followed by a slower chemical step.[95] The basicity of surface oxido-bridges may assist in proton abstraction from substrate water.[92] Najafpour *et al.* detected Mn^{II} and permanganate upon MnO_2 catalyzed water oxidation in the presence of Ce^{IV} ammonium nitrate.[227] Under-coordinated $Mn^{III}O_5$ units at amorphous boundaries were essential for high activity.[228] Nocera *et al.* obtained enhanced activity upon a phase-change of the birnessite MnO_2 precatalyst.[229] They also discovered that different mechanisms were operative, depending on pH: a one-electron one-proton PCET pathway dominated in alkaline conditions, whereas Mn^{III} disproportionation occurred in acid.[230]

Work by Zaharieva and Dau *et al.* has shown that disordering of initially more crystalline birnessite structures led to better catalytic performance. Similarly, amorphous cobalt, iron, and nickel oxides exhibited higher activities than crystalline bulk counterparts.[103,158,231] Amorphization may not be necessary in small, nanoparticulate materials, where lattice strains from rearrangements during turnover may be dissipated due to favorably large surface-to-volume ratios.

Mechanisms of cobalt oxide catalyzed water oxidation have also been studied. A possible mechanism based on reports outlined below is shown in Figure 1.10. Currently, there is broad consensus that two cofacial surface Co(O)OH moieties undergo two initial oxidations and deprotonations to generate terminal Co^{IV} oxos. Substrate water turnover likely produces a surface-bound peroxo species, which converts to a superoxo intermediate that

may be bridging. Addition of a second water molecule, together with loss of the fourth proton and electron, leads to O_2 release.

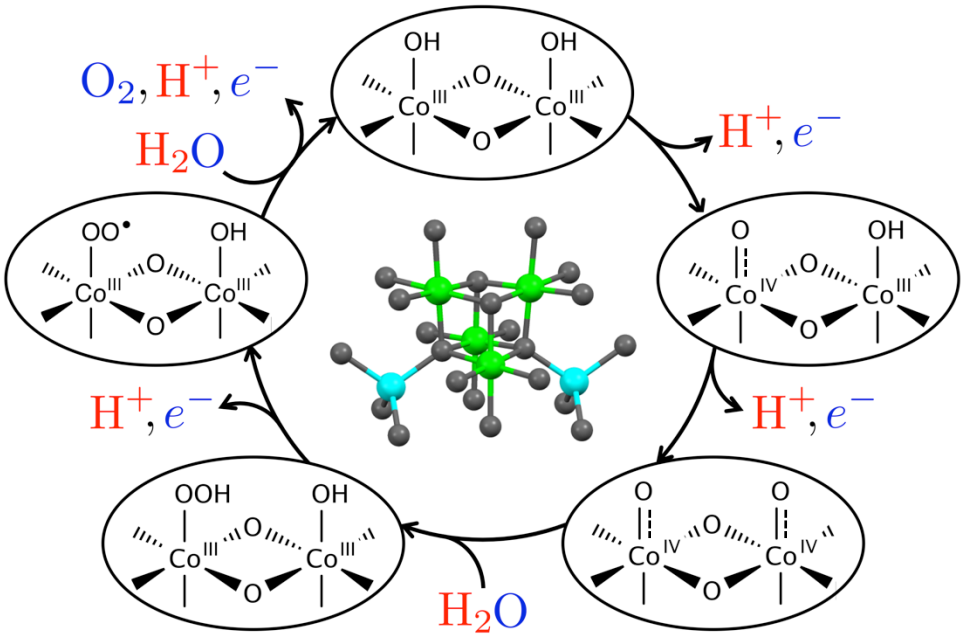

Figure 1.10. Possible mechanism of cobalt oxide catalyzed water oxidation. The Co_3O_4 structure[232] is depicted in the center; colors: Co^{II} (cyan), Co^{III} (green), O (gray).

Using DFT calculations, Van Voorhis *et al.* predicted energetics and barriers for water oxidation in a Co_4O_4 cubane cluster.[233] They suggested a mechanism in which the resting state, a (surface) μ-oxo-bridged Co^{III} hydroxide dimer, underwent metal oxidations. Radical coupling of two cofacial Co^{IV} oxo groups formed an O–O single bond. Two substrate turnover steps followed by proton transfer closed the catalytic cycle. In contrast, computations by Berlinguette and Baik *et al.* favored a mononuclear biradicaloid mechanism.[234] Siegbahn *et al.*, who performed calculations on several Co oxide model clusters, pointed out that cobalt (in contrast to manganese in PS II) prefers low-spin coupling in the relevant high oxidation states, forcing a change of electronic structure during O–O bond formation. They postulated that a Co^{IV}-oxyl radical would be needed for reactivity,[235] similar to their proposed mechanism for PS II.[201,202] Dismukes *et al.* showed that one of the studied clusters, the "Dismukes Co_4O_4 cubane", did not react with water; instead, two

hydroxide ions led to O_2 formation by an inner-sphere mechanism.[236] Water oxidation may be catalyzed by Co^{II} impurities in $Co^{III}{}_4O_4$ cubanes.[237] In other work of note, Tilley *et al.* found spectroscopic evidence for a highly oxidized terminal oxo intermediate in a Co_4O_4 cubane model compound; turnover required hydroxide.[238]

Nocera, Britt *et al.* detected Co^{IV} species by *in-situ* EPR and x-ray techniques in water oxidation catalysts generated *via* electrodeposition from aqueous solutions containing phosphate and Co^{II} (CoP_i).[107,239] Phosphorus NMR data supported the idea that electrocatalytically active CoP_i resembled an LDH with phosphate ions located in the interlamellar galleries.[240] Frei *et al.* identified oxidized Co species in Co_3O_4 nanocatalysts during turnover by *in-situ* infrared spectroscopy.[241] In other work, time-dependent redox titration experiments on CoP_i by Bard *et al.* indicated that both Co^{III} and Co^{IV} oxidized water, with pseudo-first-order rate constants of 0.19 and >2 s^{-1}, respectively.[242]

Obtaining structural and mechanistic details of heterogeneous catalysts during turnover is more straightforward with monometallic materials. But activities of multi-metallic, earth-abundant catalysts are much higher, presumably because redox potentials and catalytic pathways are fine-tuned by involving multiple metal species. For example, at a water oxidation overpotential of 280 mV, PLAL-made Co_3O_4 nanoparticles exhibited a current density of only 0.1 mA cm^{-2}, whereas [NiFe]-LDH nanosheets reached 10 mA cm^{-2}; both materials, which we investigated under virtually the same conditions in strong aqueous base on flat graphite supporting electrodes, had 100% faradaic efficiency.[115,149]

Some progress has been made in studies of even more complex materials. Bockris *et al.* investigated the mechanism of oxygen evolution on perovskites and found that OH desorption was the rate-limiting step.[243] Shao-Horn *et al.* observed amorphization of select, highly active perovskite OER catalysts.[244,245] Surface reorganization, electronic structure, and participation of lattice oxygen in the mechanism were assessed to rationalize trends in OER activities of cobaltite perovskites.[246,247]

Layered materials, especially [NiFe]-LDHs with approximately 20 to 40% Fe, have recently attracted much attention (see also previous section). They consist of slabs of $Ni^{II}(OH)_6$ edge-shared octahedra with Fe^{III} centers substituting at Ni sites. Anions in the interlamellar space between the stacked slabs balance additional positive charges that arise

from Fe^{III} occupying Ni^{II} sites; water is also intercalated.[142] Hence, Ni^{II} and Fe^{III} constitute the resting state of this catalyst. Corrigan and Boettcher *et al.* noted that Fe is required for high water oxidation activity,[118-120] suggesting that iron must be a component of the active site. Based on mechanisms occurring in nature and monometallic heterogeneous catalysts, oxidation states higher than in the resting state must be generated during turnover.

Yet Friebel and Bell *et al.* identified mononuclear Fe^{III} as the active site by DFT calculations and *operando* x-ray absorption spectroscopy (XAS) experiments on electrodeposited [$Ni^{II}Fe^{III}$]-LDH catalysts in strong aqueous base. They observed edge shapes that were unusual for octahedrally coordinated Fe^{III} and a shortening of the Fe–O distance but excluded Fe^{IV} based on their data. Instead they invoked inductive ligand effects, where oxidized Ni ions withdrew charge from O ligands shared with Fe centers, thus disfavoring Fe^{III} oxidation; a small amount of tetrahedrally coordinated Fe^{III} may also have been present.[248] Higher-valent Fe species were likely too short-lived under turnover conditions in this highly active catalyst to be detected by XAS, where the signal was overwhelmingly that of inactive Fe^{III}.

Stahl *et al.* used *operando* Mössbauer spectroscopy during water oxidation catalysis in alkaline aqueous electrolyte and identified Fe^{III} and Fe^{IV} in isotopically enriched [NiFe]-LDH materials, which were synthesized hydrothermally. Data acquisition times ranged from 18 to 24 hours. The Fe^{IV} species appeared when applied anodic potentials were high enough for water oxidation, and Fe^{IV} remained for many hours even after the applied potential was lowered below the onset of catalysis. Therefore, the detected Fe^{IV} was not deemed kinetically competent to serve as the site of water oxidation;[249] in other words, Fe^{IV} was not on path of the [NiFe]-LDH catalytic cycle.

Bard *et al.* observed "fast" and "slow" kinetics in electrodeposited [NiFe]-LDH films by surface interrogation scanning electrochemical microscopy (SI-SECM).[250] This technique allows for spatially resolved quantitative detection of redox-active surface species, without spectroscopic identification of individual intermediates. Time-dependent redox titrations revealed associated kinetics; notably, unusually high densities of catalytically participating metal sites (~300 atoms nm^{-2}) were observed, indicating fast hole conduction through

[NiFe]-LDH. For comparison, similar SI-SECM studies on Co_3O_4 and IrO_2 yielded densities of 11 and 25 nm^{-2}, respectively.[242,251]

We recently investigated the effect of interlayer anions on water oxidation activity of PLAL-made [NiFe]-LDH nanosheets in strong aqueous base (Figure 1.11). We found that carbonate replaced other interlayer anions in alkaline aqueous electrolyte in ambient air. Carbonate is of course ubiquitous and self-buffered in strong aqueous base in ambient air, as it is favored by dissolution speciation of CO_2 at high pH.[252] We discovered that carbonate-containing [NiFe]-LDH nanosheets were much more active and stable than corresponding nitrate-catalysts, which we assessed in carbonate-free electrolyte in an inert atmosphere.[253] Hence, all water oxidation electrocatalysis in high pH aqueous electrolyte in ambient air occurs in the presence of carbonate, which facilitates catalytic turnover.

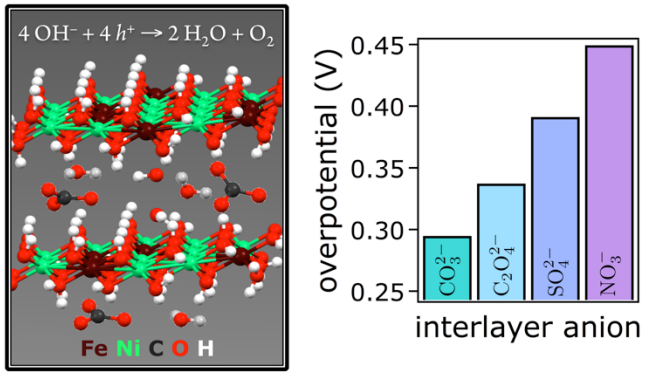

Figure 1.11. Schematic of a $[Ni^{II}Fe^{III}]$-LDH structure in strong aqueous base (left). Overpotentials of [NiFe]-LDH catalysts with the formula $[Ni_{0.78}Fe_{0.22}(OH)_2](A^{m-})_{(0.22-n)/m}(OH^-)_n \bullet xH_2O$ and different interlayer anions A^{m-} at 1.0 mA cm^{-2} (adapted from ref. 253; right).

We observed a sigmoidal dependence of OER activity on anion basicity. In plots of overpotentials, which we determined in carbonate-free electrolyte, as a function of the pK_a values of the conjugate acids of the interlayer anions, we found an apparent pK_a of (3.4±0.7) during turnover. Mechanistically, our results imply that interlayer anions act as Brønsted bases that assist deprotonation or Lewis bases, which lower oxidation potentials at the active site. The apparent pK_a of 3.4 suggests that a higher-valent metal oxo species is a catalytically active intermediate.[253]

We also have probed the likely sites of water oxidation (*i.e.* at edges or within the [NiFe]-LDH nanosheets). XPS data in combination with DFT calculations suggested that a previously unassigned N 1s species in the precatalyst, which correlated with higher water oxidation activity,[149] was nitrite bound through its N-atom to *edge-site iron*.[253] Further support for water oxidation occurring at edge sites came from our observation that catalytic activity did not correlate with basal spacings of various [NiFe]-LDH nanosheet materials, which we had prepared with different interlayer anions; slab-to-slab distances would only matter if reactants and products had to diffuse through the interlamellar galleries. Our findings indicate that edge-site Fe plays a major role in water oxidation catalysis in [NiFe]-LDH nanosheets.[253]

Why does iron improve the water oxidation activity of many mixed-metal oxide/hydroxide catalysts? Could it be related to the ease of generation of high-valent oxos on the left side of the oxo wall?[254] Is it really that simple? Surely manganese should be well suited for water oxidation if a high-valent metal-oxo center were the only criterion. But we know that inorganic and biological manganese oxo clusters differ greatly in water oxidation activity. Why is the manganese-calcium cluster in PS II so much better than purely inorganic Mn compounds? We think it likely that noncovalent peptide-cluster interactions elevate the reduction potentials of the various Ca-Mn-oxo redox states, making water oxidation energetically feasible. Of course, multiple oxidizing equivalents (holes) must be coupled to the active center (or centers) to support the removal of electrons from initially generated "oxidized-oxo" (peroxo?) intermediates to promote the reductive elimination of oxygen. In PS II, the required holes can be stored within the cluster complex itself; in a heterogeneous Fe-Ni catalyst, we suggest that hole transfer from electro- (or photo-) generated oxidized nickel centers to nearby iron active sites would produce Fe-oxos capable of oxidizing water.

In summary, water oxidation is essential for the storage of solar energy in chemical fuels. Catalysts for this critical four-electron-four-proton reaction must be highly active, robust, and based on non-precious elements to enable global scalability. Mechanistic work suggests that high-valent metal-oxo centers that are accessible at moderate anodic potentials promote electrocatalytic activity. Importantly, the availability of holes in the vicinity surface-accessible sites also enhances the performance of catalytic materials.

1.5. Parting Shots

In this chapter, we have covered recent advances in the design, synthesis, and performance of heterogeneous catalysts that potentially could be functional components of globally scalable devices for the production of solar fuels. We discussed the catalytic properties of mixed-metal materials, with emphasis on robust Ni-Fe layered double hydroxide nanosheet catalysts that exhibit exceptional activities; and we pointed out that strategic incorporation of anions into these layered catalysts improved both stability and activity. We emphasized the challenges associated with the design of acid-stable earth-abundant catalysts, and offered proposals for elements that could be incorporated in functional systems.

We highlighted how lessons from nature in combination with identification of catalytic intermediates in manmade materials aid the development of superior catalysts. We believe that further advances in this field will depend to a large measure on the success of mechanistic work, unraveling the details of the complicated proton-coupled electron transfer processes needed for efficient water oxidation.

Moving forward, we must develop innovative ways to meet our energy demand in a scalable, environmentally benign fashion. In one relevant area, we are encouraged that great strides have been made in developing potentially scalable heterogeneous water oxidation catalysts for the harnessing of solar photons to synthesize chemical fuels.

1.6. Abbreviations

AEM, alkaline exchange membrane; A^{m-}, anion; DFT, density functional theory; E^0, thermodynamic potential; E_g, bandgap; e^-, electron; en, ethylenediamine; EPR, electron paramagnetic resonance; *g*, gaseous; HER, hydrogen evolution reaction; *hv*, photon; h^+, hole; *l*, liquid, Miller index; LDH, layered double hydroxide; NHE, normal hydrogen electrode; OER, oxygen evolution reaction; PCET, proton-coupled electron transfer; PEC, photoelectrochemical; P_i, phosphate; PLAL, pulsed-laser ablation in liquids; PS II, photosystem II; RHE, reversible hydrogen electrode; SI-SECM, surface interrogation scanning electrochemical microscopy; WOC, water-oxidizing complex; XAS, x-ray absorption spectroscopy; XPS, x-ray photoelectron spectroscopy; XRD, x-ray diffraction.

1.7. References and Notes

(1) Gray, H. B. Powering the Planet with Solar Fuel. *Nature Chem.* **2009,** *1* (1), 7.

(2) Lewis, N. S.; Nocera, D. G. Powering the Planet: Chemical Challenges in Solar Energy Utilization. *Proc. Natl. Acad. Sci. U. S. A.* **2006,** *103* (43), 15729-15735.

(3) *International Energy Agency, World Energy Outlook 2015*.

(4) Lewis, N. S.; Crabtree, G. Basic Research Needs for Solar Energy Utilization: Report of the Basic Energy Sciences Workshop on Solar Energy Utilization, April 18–21, 2005. *US Department of Energy Office of Basic Energy Sciences* **2005**.

(5) Davis, S. J.; Caldeira, K.; Matthews, H. D. Future CO_2 Emissions and Climate Change from Existing Energy Infrastructure. *Science* **2010,** *329* (5997), 1330-1333.

(6) Vinyard, D. J.; Ananyev, G. M.; Dismukes, G. C. Photosystem II: the Reaction Center of Oxygenic Photosynthesis. *Annu. Rev. Biochem.* **2013,** *82*, 577-606.

(7) http://www.breakthroughenergycoalition.com

(8) Haxel, G. B.; Hedrick, J. B.; Orris, G. J.; Stauffer, P. H.; Hendley II, J. W. "Rare Earth Elements: Critical Resources for High Technology," USGS, 2002.

(9) Wood, P. M. The Potential Diagram for Oxygen at pH 7. *Biochem. J.* **1988,** *253* (1), 287-289.

(10) Britt, R. D. In *Oxygenic Photosynthesis: The Light Reactions*; Ort, D. R.;Yocum, C. F.;Heichel, I. F., Eds.; Springer Netherlands: Dordrecht, 1996.

(11) Umena, Y.; Kawakami, K.; Shen, J.-R.; Kamiya, N. Crystal Structure of Oxygen-Evolving Photosystem II at a Resolution of 1.9 Å. *Nature* **2011,** *473* (7345), 55-60.

(12) Meyer, T. J.; Huynh, M. H. V.; Thorp, H. H. The Possible Role of Proton-Coupled Electron Transfer (PCET) in Water Oxidation by Photosystem II. *Angew. Chem. Int. Edit.* **2007,** *46* (28), 5284-5304.

(13) Kok, B.; Forbush, B.; McGloin, M. Cooperation of Charges in Photosynthetic O_2 Evolution–I. A Linear Four Step Mechanism. *Photochem. Photobiol.* **1970,** *11* (6), 457-475.

(14) Brudvig, G. W. Water Oxidation Chemistry of Photosystem II. *Phil. Trans. R. Soc. Lond. B: Biol. Sci.* **2008,** *363* (1494), 1211-1219.

(15) Cukier, R. Mechanism for Proton-Coupled Electron-Transfer Reactions. *J. Phys. Chem.* **1994,** *98* (9), 2377-2381.

(16) Cukier, R. Proton-Coupled Electron Transfer through an Asymmetric Hydrogen-Bonded Interface. *J. Phys. Chem.* **1995,** *99* (43), 16101-16115.

(17) Hammes-Schiffer, S. Theoretical Perspectives on Proton-Coupled Electron Transfer Reactions. *Acc. Chem. Res.* **2001,** *34* (4), 273-281.

(18) Hammes-Schiffer, S. Introduction: Proton-Coupled Electron Transfer. *Chem. Rev.* **2010,** *110* (12), 6937-6938.

(19) Kanady, J. S.; Tsui, E. Y.; Day, M. W.; Agapie, T. A Synthetic Model of the Mn_3Ca Subsite of the Oxygen-Evolving Complex in Photosystem II. *Science* **2011,** *333* (6043), 733-736.

(20) Zhang, C.; Chen, C.; Dong, H.; Shen, J.-R.; Dau, H.; Zhao, J. A Synthetic Mn_4Ca-Cluster Mimicking the Oxygen-Evolving Center of Photosynthesis. *Science* **2015,** *348* (6235), 690-693.

(21) Borovik, A. S. Bioinspired Hydrogen Bond Motifs in Ligand Design: the Role of Noncovalent Interactions in Metal Ion Mediated Activation of Dioxygen. *Acc. Chem. Res.* **2005,** *38* (1), 54-61.

(22) Vrettos, J. S.; Limburg, J.; Brudvig, G. W. Mechanism of Photosynthetic Water Oxidation: Combining Biophysical Studies of Photosystem II with Inorganic Model Chemistry. *BBA-Bioenergetics* **2001,** *1503* (1), 229-245.

(23) Tsui, E. Y.; Tran, R.; Yano, J.; Agapie, T. Redox-Inactive Metals Modulate the Reduction Potential in Heterometallic Manganese–Oxido Clusters. *Nature Chem.* **2013,** *5* (4), 293-299.

(24) McKone, J. R.; Lewis, N. S.; Gray, H. B. Will Solar-Driven Water-Splitting Devices See the Light of Day? *Chem. Mater.* **2013,** *26* (1), 407-414.

(25) Parkinson, B. On the Efficiency and Stability of Photoelectrochemical Devices. *Acc. Chem. Res.* **1984,** *17* (12), 431-437.

(26) Khaselev, O.; Turner, J. A. A Monolithic Photovoltaic-Photoelectrochemical Device for Hydrogen Production via Water Splitting. *Science* **1998,** *280* (5362), 425-427.

(27) Newman, J.; Hoertz, P. G.; Bonino, C. A.; Trainham, J. A. Review: an Economic Perspective on Liquid Solar Fuels. *J. Electrochem. Soc.* **2012,** *159* (10), A1722-A1729.

(28) Tachibana, Y.; Vayssieres, L.; Durrant, J. R. Artificial Photosynthesis for Solar Water-Splitting. *Nat. Photonics* **2012,** *6* (8), 511-518.

(29) Osterloh, F. E. Inorganic Nanostructures for Photoelectrochemical and Photocatalytic Water Splitting. *Chem. Soc. Rev.* **2013,** *42* (6), 2294-2320.

(30) Pinaud, B. A.; Benck, J. D.; Seitz, L. C.; Forman, A. J.; Chen, Z.; Deutsch, T. G.; James, B. D.; Baum, K. N.; Baum, G. N.; Ardo, S.et al. Technical and Economic Feasibility of Centralized Facilities for Solar Hydrogen Production via Photocatalysis and Photoelectrochemistry. *Energy Environ. Sci.* **2013,** *6* (7), 1983-2002.

(31) Döscher, H.; Geisz, J. F.; Deutsch, T. G.; Turner, J. A. Sunlight Absorption in Water–Efficiency and Design Implications for Photoelectrochemical Devices. *Energy Environ. Sci.* **2014,** *7* (9), 2951-2956.

(32) Gu, S.; Xu, B.; Yan, Y. Electrochemical Energy Engineering: a New Frontier of Chemical Engineering Innovation. *Annu. Rev. Chem. Biomol. Eng.* **2014,** *5*, 429-454.

(33) Luo, J.; Im, J.-H.; Mayer, M. T.; Schreier, M.; Nazeeruddin, M. K.; Park, N.-G.; Tilley, S. D.; Fan, H. J.; Grätzel, M. Water Photolysis at 12.3% Efficiency via Perovskite Photovoltaics and Earth-Abundant Catalysts. *Science* **2014,** *345* (6204), 1593-1596.

(34) Chen, Y.; Sun, K.; Audesirk, H.; Xiang, C.; Lewis, N. S. A Quantitative Analysis of the Efficiency of Solar-Driven Water-Splitting Device Designs Based on Tandem Photoabsorbers Patterned with Islands of Metallic Electrocatalysts. *Energy Environ. Sci.* **2015,** *8* (6), 1736-1747.

(35) Dumortier, M.; Haussener, S. Design Guidelines for Concentrated Photo-Electrochemical Water Splitting Devices Based on Energy and Greenhouse Gas Yield Ratios. *Energy Environ. Sci.* **2015,** *8* (11), 3069-3082.

(36) Verlage, E.; Hu, S.; Liu, R.; Jones, R. J. R.; Sun, K.; Xiang, C.; Lewis, N. S.; Atwater, H. A. A Monolithically Integrated, Intrinsically Safe, 10% Efficient, Solar-Driven Water-Splitting System Based on Active, Stable Earth-Abundant Electrocatalysts in Conjunction with Tandem III-V Light Absorbers Protected by Amorphous TiO_2 Films. *Energy Environ. Sci.* **2015,** *8* (11), 3166-3172.

(37) Doscher, H.; Young, J. L.; Geisz, J. F.; Turner, J. A.; Deutsch, T. G. Solar-to-Hydrogen Efficiency: Shining Light on Photoelectrochemical Device Performance. *Energy Environ. Sci.* **2016,** *9* (1), 74-80.

(38) Kärkäs, M. D.; Verho, O.; Johnston, E. V.; Åkermark, B. Artificial Photosynthesis: Molecular Systems for Catalytic Water Oxidation. *Chem. Rev.* **2014,** *114* (24), 11863-12001.

(39) Blakemore, J. D.; Crabtree, R. H.; Brudvig, G. W. Molecular Catalysts for Water Oxidation. *Chem. Rev.* **2015,** *115* (23), 12974-13005.

(40) Kärkäs, M.; Åkermark, B. Water Oxidation using Earth-Abundant Transition Metal Catalysts: Opportunities and Challenges. *Dalton Trans.* **2016,** *45* (37), 14421-14461.

(41) Pourbaix, M. *Atlas of Electrochemical Equilibria in Aqueous Solutions*; Pergamon Press: New York, 1966.

(42) Leng, Y.; Chen, G.; Mendoza, A. J.; Tighe, T. B.; Hickner, M. A.; Wang, C.-Y. Solid-State Water Electrolysis with an Alkaline Membrane. *J. Am. Chem. Soc.* **2012,** *134* (22), 9054-9057.

(43) Varcoe, J. R.; Atanassov, P.; Dekel, D. R.; Herring, A. M.; Hickner, M. A.; Kohl, P. A.; Kucernak, A. R.; Mustain, W. E.; Nijmeijer, K.; Scott, K. Anion-Exchange Membranes in Electrochemical Energy Systems. *Energy Environ. Sci.* **2014,** *7* (10), 3135-3191.

(44) Walter, M. G.; Warren, E. L.; McKone, J. R.; Boettcher, S. W.; Mi, Q.; Santori, E. A.; Lewis, N. S. Solar Water Splitting Cells. *Chem. Rev.* **2010,** *110* (11), 6446-6473.

(45) Load changes, as they occur in sun-light-driven devices because of the diurnal nature of solar illumination, will be another major consideration regarding optimal pH conditions.

(46) Kim, J.; Yin, X.; Tsao, K.-C.; Fang, S.; Yang, H. $Ca_2Mn_2O_5$ as Oxygen-Deficient Perovskite Electrocatalyst for Oxygen Evolution Reaction. *J. Am. Chem. Soc.* **2014,** *136* (42), 14646-14649.

(47) Diaz-Morales, O.; Ledezma-Yanez, I.; Koper, M. T.; Calle-Vallejo, F. Guidelines for the Rational Design of Ni-Based Double Hydroxide Electrocatalysts for the Oxygen Evolution Reaction. *ACS Catal.* **2015,** *5* (9), 5380-5387.

(48) Bockris, J. O.; Otagawa, T. The Electrocatalysis of Oxygen Evolution on Perovskites. *J. Electrochem. Soc.* **1984,** *131* (2), 290-302.

(49) Mauritz, K. A.; Moore, R. B. State of Understanding of Nafion. *Chem. Rev.* **2004,** *104* (10), 4535-4586.

(50) Carmo, M.; Fritz, D. L.; Mergel, J.; Stolten, D. A Comprehensive Review on PEM Water Electrolysis. *Int. J. Hydrogen Energy* **2013,** *38* (12), 4901-4934.

(51) Harriman, A.; Pickering, I. J.; Thomas, J. M.; Christensen, P. A. Metal Oxides as Heterogeneous Catalysts for Oxygen Evolution under Photochemical Conditions. *J. Chem. Soc., Faraday Trans. I* **1988,** *84* (8), 2795-2806.

(52) Chen, X.; Chen, G.; Yue, P. L. Stable $Ti/IrO_x–Sb_2O_5–SnO_2$ Anode for O_2 Evolution with Low Ir Content. *J. Phys. Chem. B* **2001,** *105* (20), 4623-4628.

(53) Blakemore, J. D.; Schley, N. D.; Olack, G. W.; Incarvito, C. D.; Brudvig, G. W.; Crabtree, R. H. Anodic Deposition of a Robust Iridium-Based Water-Oxidation Catalyst from Organometallic Precursors. *Chem. Sci.* **2011,** *2* (1), 94-98.

(54) Schley, N. D.; Blakemore, J. D.; Subbaiyan, N. K.; Incarvito, C. D.; D'Souza, F.; Crabtree, R. H.; Brudvig, G. W. Distinguishing Homogeneous from Heterogeneous Catalysis in Electrode-Driven Water Oxidation with Molecular Iridium Complexes. *J. Am. Chem. Soc.* **2011,** *133* (27), 10473-10481.

(55) Frame, F. A.; Townsend, T. K.; Chamousis, R. L.; Sabio, E. M.; Dittrich, T.; Browning, N. D.; Osterloh, F. E. Photocatalytic Water Oxidation with Nonsensitized IrO_2 Nanocrystals under Visible and UV Light. *J. Am. Chem. Soc.* **2011,** *133* (19), 7264-7267.

(56) Wang, C.; Xie, Z.; deKrafft, K. E.; Lin, W. Doping Metal–Organic Frameworks for Water Oxidation, Carbon Dioxide Reduction, and Organic Photocatalysis. *J. Am. Chem. Soc.* **2011,** *133* (34), 13445-13454.

(57) Fujishima, A.; Honda, K. Electrochemical Photolysis of Water at a Semiconductor Electrode. *Nature* **1972,** *238* (5358), 37-38.

(58) Walsh, A.; Yan, Y.; Huda, M. N.; Al-Jassim, M. M.; Wei, S.-H. Band Edge Electronic Structure of $BiVO_4$: Elucidating the Role of the Bi s and V d Orbitals. *Chem. Mater.* **2009,** *21* (3), 547-551.

(59) Prévot, M. S.; Sivula, K. Photoelectrochemical Tandem Cells for Solar Water Splitting. *J. Phys. Chem. C* **2013,** *117* (35), 17879-17893.

(60) Liu, M.; Nam, C.-Y.; Black, C. T.; Kamcev, J.; Zhang, L. Enhancing Water Splitting Activity and Chemical Stability of Zinc Oxide Nanowire Photoanodes with Ultrathin Titania Shells. *J. Phys. Chem. C* **2013,** *117* (26), 13396-13402.

(61) Kato, H.; Asakura, K.; Kudo, A. Highly Efficient Water Splitting into H_2 and O_2 over Lanthanum-Doped $NaTaO_3$ Photocatalysts with High Crystallinity and Surface Nanostructure. *J. Am. Chem. Soc.* **2003,** *125* (10), 3082-3089.

(62) Lau, L. C.; Lee, K. T. The Effect of Band Engineering of Semiconductors on Photocatalytic Water Splitting: A Review. *IJRET* **2013,** *2* (11), 195-206.

(63) Mi, Q.; Zhanaidarova, A.; Brunschwig, B. S.; Gray, H. B.; Lewis, N. S. A Quantitative Assessment of the Competition between Water and Anion Oxidation at WO_3 Photoanodes in Acidic Aqueous Electrolytes. *Energy Environ. Sci.* **2012,** *5* (2), 5694-5700.

(64) Miseki, Y.; Sayama, K. High-Efficiency Water Oxidation and Energy Storage Utilizing Various Reversible Redox Mediators under Visible Light over Surface-Modified WO_3. *RSC Adv.* **2014,** *4* (16), 8308-8316.

(65) Kawasaki, S.; Nakatsuji, K.; Yoshinobu, J.; Komori, F.; Takahashi, R.; Lippmaa, M.; Mase, K.; Kudo, A. Epitaxial Rh-Doped $SrTiO_3$ Thin Film Photocathode for Water Splitting under Visible Light Irradiation. *Appl. Phys. Lett.* **2012,** *101* (3), 033910.

(66) Bolton, J. R.; Strickler, S. J.; Connolly, J. S. Limiting and Realizable Efficiencies of Solar Photolysis of Water. *Nature* **1985,** *316* (6028), 495-500.

(67) Sakthivel, S.; Janczarek, M.; Kisch, H. Visible Light Activity and Photoelectrochemical Properties of Nitrogen-Doped TiO_2. *J. Phys. Chem. B* **2004,** *108* (50), 19384-19387.

(68) Mi, Q.; Ping, Y.; Li, Y.; Cao, B.; Brunschwig, B. S.; Khalifah, P. G.; Galli, G. A.; Gray, H. B.; Lewis, N. S. Thermally Stable N_2-Intercalated WO_3 Photoanodes for Water Oxidation. *J. Am. Chem. Soc.* **2012,** *134* (44), 18318-18324.

(69) A TiO_2 bandgap of 2.9 eV is still too large for efficient light absorption; and tungsten oxide is not stable in alkaline media in which highly active, earth-abundant water oxidation catalysts operate.

(70) Suntivich, J.; May, K. J.; Gasteiger, H. A.; Goodenough, J. B.; Shao-Horn, Y. A Perovskite Oxide Optimized for Oxygen Evolution Catalysis from Molecular Orbital Principles. *Science* **2011,** *334* (6061), 1383-1385.

(71) Liu, H.; Moré, R.; Grundmann, H.; Cui, C.; Erni, R.; Patzke, G. R. Promoting Photochemical Water Oxidation with Metallic Band Structures. *J. Am. Chem. Soc.* **2016,** *138* (5), 1527-1535.

(72) Hildebrandt, N. C.; Soldat, J.; Marschall, R. Layered Perovskite Nanofibers via Electrospinning for Overall Water Splitting. *Small* **2015,** *11* (17), 2051-2057.

(73) Park, Y.; McDonald, K. J.; Choi, K.-S. Progress in Bismuth Vanadate Photoanodes for use in Solar Water Oxidation. *Chem. Soc. Rev.* **2013,** *42* (6), 2321-2337.

(74) Abdi, F. F.; Firet, N.; Dabirian, A.; van de Krol, R. Spray-Deposited Co-Pi Catalyzed $BiVO_4$: a Low-Cost Route towards Highly Efficient Photoanodes. *MRS Proceedings* **2012,** *1446*, 7-12.

(75) Kudo, A.; Omori, K.; Kato, H. A Novel Aqueous Process for Preparation of Crystal Form-Controlled and Highly Crystalline $BiVO_4$ Powder from Layered Vanadates at Room Temperature and Its Photocatalytic and Photophysical Properties. *J. Am. Chem. Soc.* **1999,** *121* (49), 11459-11467.

(76) Tokunaga, S.; Kato, H.; Kudo, A. Selective Preparation of Monoclinic and Tetragonal $BiVO_4$ with Scheelite Structure and Their Photocatalytic Properties. *Chem. Mater.* **2001,** *13* (12), 4624-4628.

(77) Kudo, A.; Ueda, K.; Kato, H.; Mikami, I. Photocatalytic O_2 Evolution under Visible Light Irradiation on $BiVO_4$ in Aqueous $AgNO_3$ Solution. *Catal. Lett.* **1998,** *53* (3-4), 229-230.

(78) Abdi, F. F.; Firet, N.; van de Krol, R. Efficient $BiVO_4$ Thin Film Photoanodes Modified with Cobalt Phosphate Catalyst and W-doping. *ChemCatChem* **2013,** *5* (2), 490-496.

(79) Alarcon-Llado, E.; Chen, L.; Hettick, M.; Mashouf, N.; Lin, Y.; Javey, A.; Ager, J. W. $BiVO_4$ Thin Film Photoanodes Grown by Chemical Vapor Deposition. *Phys. Chem. Chem. Phys.* **2014,** *16* (4), 1651-1657.

(80) Berglund, S. P.; Flaherty, D. W.; Hahn, N. T.; Bard, A. J.; Mullins, C. B. Photoelectrochemical Oxidation of Water Using Nanostructured $BiVO_4$ Films. *J. Phys. Chem. C* **2011,** *115* (9), 3794-3802.

(81) Chen, L.; Alarcón-Lladó, E.; Hettick, M.; Sharp, I. D.; Lin, Y.; Javey, A.; Ager, J. W. Reactive Sputtering of Bismuth Vanadate Photoanodes for Solar Water Splitting. *J. Phys. Chem. C* **2013,** *117* (42), 21635-21642.

(82) Choi, S. K.; Choi, W.; Park, H. Solar Water Oxidation using Nickel-Borate Coupled $BiVO_4$ Photoelectrodes. *Phys. Chem. Chem. Phys.* **2013,** *15* (17), 6499-6507.

(83) Jeong, H. W.; Jeon, T. H.; Jang, J. S.; Choi, W.; Park, H. Strategic Modification of $BiVO_4$ for Improving Photoelectrochemical Water Oxidation Performance. *J. Phys. Chem. C* **2013,** *117* (18), 9104-9112.

(84) Kim, T. W.; Choi, K. S. Nanoporous $BiVO_4$ Photoanodes with Dual-Layer Oxygen Evolution Catalysts for Solar Water Splitting. *Science* **2014,** *343* (6174), 990-994.

(85) Sayama, K.; Wang, N.; Miseki, Y.; Kusama, H.; Onozawa-Komatsuzaki, N.; Sugihara, H. Effect of Carbonate Ions on the Photooxidation of Water over Porous $BiVO_4$ Film Photoelectrode under Visible Light. *Chem. Lett.* **2010,** *39* (1), 17-19.

(86) Seabold, J. A.; Choi, K.-S. Efficient and Stable Photo-Oxidation of Water by a Bismuth Vanadate Photoanode Coupled with an Iron Oxyhydroxide Oxygen Evolution Catalyst. *J. Am. Chem. Soc.* **2012,** *134* (4), 2186-2192.

(87) Su, J.; Guo, L.; Yoriya, S.; Grimes, C. A. Aqueous Growth of Pyramidal-Shaped $BiVO_4$ Nanowire Arrays and Structural Characterization: Application to Photoelectrochemical Water Splitting. *Cryst. Growth Des.* **2009,** *10* (2), 856-861.

(88) Sinclair, T. S.; Hunter, B. M.; Winkler, J. R.; Gray, H. B.; Müller, A. M. Factors Affecting Bismuth Vanadate Photoelectrochemical Performance. *Mater. Horiz.* **2015,** *2* (3), 330-337.

(89) Morita, M.; Iwakura, C.; Tamura, H. The Anodic Characteristics of Manganese Dioxide Electrodes Prepared by Thermal Decomposition of Manganese Nitrate. *Electrochim. Acta* **1977,** *22* (4), 325-328.

(90) Jiao, F.; Frei, H. Nanostructured Manganese Oxide Clusters Supported on Mesoporous Silica as Efficient Oxygen-Evolving Catalysts. *Chem. Commun.* **2010,** *46* (17), 2920-2922.

(91) Pinaud, B. A.; Chen, Z.; Abram, D. N.; Jaramillo, T. F. Thin Films of Sodium Birnessite-Type MnO_2: Optical Properties, Electronic Band Structure, and Solar Photoelectrochemistry. *J. Phys. Chem. C* **2011,** *115* (23), 11830-11838.

(92) Wiechen, M.; Zaharieva, I.; Dau, H.; Kurz, P. Layered Manganese Oxides for Water-Oxidation: Alkaline Earth Cations Influence Catalytic Activity in a Photosystem II-Like Fashion. *Chem. Sci.* **2012,** *3* (7), 2330-2339.

(93) Pokhrel, R.; Goetz, M. K.; Shaner, S. E.; Wu, X.; Stahl, S. S. The "Best Catalyst" for Water Oxidation Depends on the Oxidation Method Employed: A Case Study of Manganese Oxides. *J. Am. Chem. Soc.* **2015,** *137* (26), 8384-8387.

(94) Najafpour, M. M.; Sedigh, D. J. Water Oxidation by Manganese Oxides, a New Step towards a Complete Picture: Simplicity is the Ultimate Sophistication. *Dalton Trans.* **2013,** *42* (34), 12173-12178.

(95) Zaharieva, I.; Chernev, P.; Risch, M.; Klingan, K.; Kohlhoff, M.; Fischer, A.; Dau, H. Electrosynthesis, Functional, and Structural Characterization of a Water-Oxidizing Manganese Oxide. *Energy Environ. Sci.* **2012,** *5* (5), 7081-7089.

(96) Najafpour, M. M.; Ehrenberg, T.; Wiechen, M.; Kurz, P. Calcium Manganese(III) Oxides ($CaMn_2O_4 \cdot xH_2O$) as Biomimetic Oxygen-Evolving Catalysts. *Angew. Chem. Int. Edit.* **2010,** *49* (12), 2233-2237.

(97) Kurz, P.; Berggren, G.; Anderlund, M. F.; Styring, S. Oxygen Evolving Reactions Catalysed by Synthetic Manganese Complexes: A Systematic Screening. *Dalton Trans.* **2007,** *2007* (38), 4258-4261.

(98) Najafpour, M.; Moghaddam, A. N.; Dau, H.; Zaharieva, I. Fragments of Layered Manganese Oxide are the Real Water Oxidation Catalyst after Transformation of Molecular Precursor on Clay. *J. Am. Chem. Soc.* **2014,** *136* (20), 7245-7248.

(99) Gorlin, Y.; Jaramillo, T. F. A Bifunctional Nonprecious Metal Catalyst for Oxygen Reduction and Water Oxidation. *J. Am. Chem. Soc.* **2010,** *132* (39), 13612-13614.

(100) Gorlin, Y.; Lassalle-Kaiser, B.; Benck, J. D.; Gul, S.; Webb, S. M.; Yachandra, V. K.; Yano, J.; Jaramillo, T. F. In Situ X-ray Absorption Spectroscopy Investigation of a Bifunctional Manganese Oxide Catalyst with High Activity for Electrochemical Water Oxidation and Oxygen Reduction. *J. Am. Chem. Soc.* **2013,** *135* (23), 8525-8534.

(101) Turner, J.; Hendewerk, M.; Parmeter, J.; Neiman, D.; Somorjai, G. The Characterization of Doped Iron Oxide Electrodes for the Photodissociation of Water Stability, Optical, and Electronic Properties. *J. Electrochem. Soc.* **1984,** *131* (8), 1777-1783.

(102) Joly, A. G.; Williams, J. R.; Chambers, S. A.; Xiong, G.; Hess, W. P.; Laman, D. M. Carrier Dynamics in α-Fe2O3 (0001) Thin Films and Single Crystals Probed by Femtosecond Transient Absorption and Reflectivity. *J. Appl. Phys.* **2006,** *99* (5), 053521.

(103) Smith, R. D. L.; Prévot, M. S.; Fagan, R. D.; Zhang, Z.; Sedach, P. A.; Siu, M. K. J.; Trudel, S.; Berlinguette, C. P. Photochemical Route for Accessing Amorphous Metal Oxide Materials for Water Oxidation Catalysis. *Science* **2013,** *340* (6128), 60-63.

(104) Cesar, I.; Kay, A.; Gonzalez Martinez, J. A.; Grätzel, M. Translucent Thin Film Fe_2O_3 Photoanodes for Efficient Water Splitting by Sunlight: Nanostructure-Directing Effect of Si-Doping. *J. Am. Chem. Soc.* **2006,** *128* (14), 4582-4583.

(105) Lyons, M. E. G.; Brandon, M. P. The Oxygen Evolution Reaction on Passive Oxide Covered Transition Metal Electrodes in Aqueous Alkaline Solution. Part III - Iron. *Int. J. Electrochem. Sci.* **2008,** *3* (12), 1463-1503.

(106) Kanan, M. W.; Nocera, D. G. In Situ Formation of an Oxygen-Evolving Catalyst in Neutral Water Containing Phosphate and Co^{2+}. *Science* **2008,** *321* (5892), 1072-1075.

(107) McAlpin, J. G.; Surendranath, Y.; Dincă, M.; Stich, T. A.; Stoian, S. A.; Casey, W. H.; Nocera, D. G.; Britt, R. D. EPR Evidence for Co(IV) Species Produced During Water Oxidation at Neutral pH. *J. Am. Chem. Soc.* **2010,** *132* (20), 6882-6883.

(108) Risch, M.; Klingan, K.; Ringleb, F.; Chernev, P.; Zaharieva, I.; Fischer, A.; Dau, H. Water Oxidation by Electrodeposited Cobalt Oxides—Role of Anions and Redox-Inert Cations in Structure and Function of the Amorphous Catalyst. *ChemSusChem* **2012,** *5* (3), 542-549.

(109) El Wakkad, S. E. S.; Hickling, A. The Anodic Behaviour of Metals. Part VI.-Cobalt. *T. Faraday Soc.* **1950,** *46* (0), 820-824.

(110) Pandey, A. D.; Jia, C.; Schmidt, W.; Leoni, M.; Schwickardi, M.; Schüth, F.; Weidenthaler, C. Size-Controlled Synthesis and Microstructure Investigation of Co_3O_4 Nanoparticles for Low-Temperature CO Oxidation. *J. Phys. Chem. C* **2012,** *116* (36), 19405-19412.

(111) Gardner, G. P.; Go, Y. B.; Robinson, D. M.; Smith, P. F.; Hadermann, J.; Abakumov, A.; Greenblatt, M.; Dismukes, G. C. Structural Requirements in Lithium Cobalt Oxides for the Catalytic Oxidation of Water. *Angew. Chem. Int. Edit.* **2012,** *51* (7), 1616-1619.

(112) Song, F.; Hu, X. Ultrathin Cobalt–Manganese Layered Double Hydroxide Is an Efficient Oxygen Evolution Catalyst. *J. Am. Chem. Soc.* **2014,** *136* (47), 16481-16484.

(113) Grzelczak, M.; Zhang, J.; Pfrommer, J.; Hartmann, J.; Driess, M.; Antonietti, M.; Wang, X. Electro- and Photochemical Water Oxidation on Ligand-free Co_3O_4 Nanoparticles with Tunable Sizes. *ACS Catal.* **2013,** *3* (3), 383-388.

(114) Lyons, M. E. G.; Brandon, M. P. The Oxygen Evolution Reaction on Passive Oxide Covered Transition Metal Electrodes in Aqueous Alkaline Solution. Part II - Cobalt. *Int. J. Electrochem. Sci.* **2008,** *3* (12), 1425-1462.

(115) Blakemore, J. D.; Gray, H. B.; Winkler, J. R.; Müller, A. M. Co_3O_4 Nanoparticle Water-Oxidation Catalysts Made by Pulsed-Laser Ablation in Liquids. *ACS Catal.* **2013,** *3* (11), 2497-2500.

(116) Bode, H.; Dehmelt, K.; Witte, J. Zur Kenntnis der Nickelhydroxidelektrode—I. Über das Nickel(II)-Hydroxidhydrat. *Electrochim. Acta* **1966,** *11* (8), 1079-IN1071.

(117) Oliva, P.; Leonardi, J.; Laurent, J. F.; Delmas, C.; Braconnier, J. J.; Figlarz, M.; Fievet, F.; Guibert, A. d. Review of the Structure and the Electrochemistry of Nickel Hydroxides and Oxy-Hydroxides. *J. Power Sources* **1982,** *8* (2), 229-255.

(118) Młynarek, G.; Paszkiewicz, M.; Radniecka, A. The Effect of Ferric Ions on the Behaviour of a Nickelous Hydroxide Electrode. *J. Appl. Electrochem.* **1984,** *14* (2), 145-149.

(119) Corrigan, D. A. The Catalysis of the Oxygen Evolution Reaction by Iron Impurities in Thin Film Nickel Oxide Electrodes. *J. Electrochem. Soc.* **1987,** *134* (2), 377-384.

(120) Trotochaud, L.; Young, S. L.; Ranney, J. K.; Boettcher, S. W. Nickel-Iron Oxyhydroxide Oxygen-Evolution Electrocatalysts: the Role of Intentional and Incidental Iron Incorporation. *J. Am. Chem. Soc.* **2014,** *136* (18), 6744-6753.

(121) Lyons, M. E. G.; Brandon, M. P. The Oxygen Evolution Reaction on Passive Oxide Covered Transition Metal Electrodes in Aqueous Alkaline Solution. Part I - Nickel. *Int. J. Electrochem. Sci.* **2008,** *3* (12), 1386-1424.

(122) Chen, J. Y. C.; Miller, J. T.; Gerken, J. B.; Stahl, S. S. Inverse Spinel $NiFeAlO_4$ as a Highly Active Oxygen Evolution Electrocatalyst: Promotion of Activity by a Redox-Inert Metal Ion. *Energy Environ. Sci.* **2014,** *7* (4), 1382-1386.

(123) Niedbala, J.; Budniok, A.; Surowka, J.; Gierlotka, D. Electrolytic Oxygen Evolution on Ni-P-Sc_2O_3 Composite Layers. *Thin Solid Films* **1996,** *287* (1-2), 164-168.

(124) Liu, H.; Nakamura, R.; Nakato, Y. Bismuth-Copper Vanadate $BiCu_2VO_6$ as a Novel Photocatalyst for Efficient Visible-Light-Driven Oxygen Evolution. *ChemPhysChem* **2005,** *6* (12), 2499-2502.

(125) Xing, M.; Kong, L.-B.; Liu, M.-C.; Liu, L.-Y.; Kang, L.; Luo, Y.-C. Cobalt Vanadate as Highly Active, Stable, Noble Metal-Free Oxygen Evolution Electrocatalyst. *J. Mater. Chem. A* **2014,** *2* (43), 18435-18443.

(126) Aki, S. N. V. K.; Ding, Z.-Y.; Abraham, M. A. Catalytic Supercritical Water Oxidation: Stability of Cr_2O_3 Catalyst. *AIChE J.* **1996,** *42* (7), 1995-2004.

(127) Soldat, J.; Busser, G. W.; Muhler, M.; Wark, M. Cr_2O_3 Nanoparticles on $Ba_5Ta_4O_{15}$ as a Noble-Metal-Free Oxygen Evolution Co-Catalyst for Photocatalytic Overall Water Splitting. *ChemCatChem* **2016,** *8* (1), 153-156.

(128) Du, J.; Chen, Z.; Ye, S.; Wiley, B. J.; Meyer, T. J. Copper as a Robust and Transparent Electrocatalyst for Water Oxidation. *Angew. Chem., Int. Ed.* **2015,** *54* (7), 2073-2078.